Physics – Uspekhi **61** (2) 133 – 156 (2018)

REVIEWS OF TOPICAL PROBLEMS

PACS numbers: **68.65. – k**, 73.20.Mf, **78.67. – n**

1000th issue of *Uspekhi Fizicheskikh Nauk* journal

Optics and spectroscopy of a single plasmonic nanostructure

V I Balykin, P N Melentiev

DOI: https://doi.org/10.3367/UFNe.2017.06.038163

Contents

Abstract. We review the interaction of laser light with a single plasmonic nanostructure. Until recently, the extremely weak optical response of a single nanostructure had only allowed spectroscopic research on ensembles of nanoparticles, where both structural and material parameters vary from one nanoparticle to another and the optical response is therefore averaged over the ensemble. Measurements at the level of a single nanostructure provide an effective tool for investigating the fundamental optical and spectroscopic properties of nanostructures, allowing insight into the mechanisms of elementary physical processes and permitting one to avoid the averaging procedure with the inevitable loss of physical information. The diverse range of linear-interaction optical phenomena occurring in a weak light field is reviewed and nonlinear interaction with high-intensity radiation is discussed.

Keywords: nanoplasmonics, single plasmonic nanostructures, nonlinear nanoplasmonics, applications of single plasmonic nanostructures

V I Balykin, P N Melentiev Institute of Spectroscopy,
Russian Academy of Sciences,
ul. Fizicheskaya 5, 108840 Troitsk, Moscow, Russian Federation
Tel. +7 (495) 851 02 33. Fax +7 (495) 851 08 86
E-mail: balykin@isan.troitsk.ru, melentiev@isan.troitsk.ru

Received 25 October 2016, revised 23 June 2017
Uspekhi Fizicheskikh Nauk **188** (2) 143 – 168 (2018)
DOI: https://doi.org/10.3367/UFNr.2017.06.038163
Translated by M N Sapozhnikov; edited by A M Semikhatov

1. Introduction

Because of the extremely weak optical response of a single nanostructure, fundamental research in nanoplasmonics was performed until recently with ensembles of nanoparticles (typically containing $10^4 - 10^6$ nanostructures) [1, 2]. Both structural and material parameters in ensembles of nanoparticles vary, as a rule, from one nanoparticle to another, and therefore the optical response is averaged over the ensemble.

Despite the impressive advances of modern nanotechnology (electron and ion lithography, methods of ion optics, etc.), the creation of nanostructures with identical geometrical and physical parameters remains an unsolved problem. On the other hand, state-of-the-art experimental optical and spectroscopic technologies allow studying single atoms and molecules [3, 4]. Measurements of *single* nanostructures can be efficiently used for studying fundamental optical and spectroscopic properties to determine mechanisms of elementary physical processes by avoiding ensemble averaging, which inevitably leads to the loss of physical information on the parameters of nanoparticles, such as the absorption cross section, the quantum yield of emission, and the polarization anisotropy of emission and absorption.

Optical and spectroscopic properties of nanostructures are directly related to their internal characteristics (composition, structure, size, and shape) and their environment (adsorbed molecules, matrices, and other particles). Therefore, by varying the internal parameters of a nanoparticle and its environment, we can control the optical and spectroscopic properties of nanostructures. All this makes the development of optical methods for detecting and characterizing individual

nanostructures the central direction in fundamental and applied nanotechnology investigations.

Interest in single plasmonic nanostructures arose, in particular, due to the possibility of using them in schemes being developed for all-optical data control and information transfer [5], where plasmonic nanoparticles provide detection and control of an optical signal at the nanometer spatial scale with subfemtosecond time resolution [6]. However, modern studies have shown that the possibilities of using a single plasmonic nanostructure are considerably wider. They also include investigations of the optical properties of metals at the nanometer scale and the structure of their electron levels, including quantum effects and different types of optical nonlinear interactions. A single plasmonic nanostructure can be used for studying the temporal properties of pulsed laser radiation, creating optical tweezers, and many other applications.

The aim of this review is to consider the interaction of laser light with single plasmonic nanostructures, a variety of optical phenomena involved in this interaction, and the possibilities of their practical applications. We consider the case of weak light fields (linear optical interaction) and also interaction with high-intensity radiation (nonlinear optical interaction).

The review is organized as follows. In Section 2, we consider theoretical foundations of the interaction of light with nanostructures and optical properties of single plasmonic nanostructures. In Sections 3 and 4, the properties of strong nonlinear optical interactions of single plasmonic nanostructures with laser radiation are discussed. In Section 5, some practical applications of single plasmonic nanostructures are presented. In the conclusion, we assess the scientific importance of using single plasmonic nanostructures in modern optical laboratories and outline their practical applications.

2. Optical properties of a single nanostructure

2.1 Electromagnetic properties of metal nanoparticles

The optics of metal nanostructures are quite well described in the framework of classical electrodynamics based on Maxwell's equations. It is generally accepted that Maxwell's equations can be applied to nanoparticles down to 1 nm in size. In general, the optical response of metals is nonlocal in space and time and is also anisotropic. The spatial nonlocality can be very strong for metals, but the local approximation is quite accurate when the wavelength λ in a material greatly exceeds all other characteristic sizes (such as the electron mean free path). The local approximation is usually highly accurate in a broad spectral range, including the UV range. In this approximation, the relation between the polarization and the field has the form [7]

$$\mathbf{P}(\mathbf{r},t)=\int \mathrm{d}t'\,\chi(\mathbf{r};t-t')\,\mathbf{E}(\mathbf{r},t')\,, \tag{1}$$

where χ is the scalar dielectric perceptibility. By applying the Fourier transformation to (1), we obtain the relation between the frequency components of the polarization and field,

$$\tilde{P}(\mathbf{r},\omega)=\tilde{\chi}(\mathbf{r},\omega)\,\tilde{E}(\mathbf{r},\omega)\,, \tag{2}$$

$$\tilde{D}(\mathbf{r},\omega)=\tilde{\varepsilon}(\mathbf{r},\omega)\,\tilde{E}(\mathbf{r},\omega)\,, \tag{3}$$

where $\tilde{\varepsilon}(\mathbf{r},\omega)$ is the complex permittivity of the medium. The dielectric perceptibility and permittivity of the medium are related as

$$\tilde{\varepsilon}(\mathbf{r},\omega)=1+4\pi\tilde{\chi}(\mathbf{r},\omega)\,. \tag{4}$$

Thus, determining the optical response of a metal nanostructure reduces to calculating and measuring the permittivity of the medium.

2.1.1 Permittivity of a metal. The Drude model. Optical properties of metals are largely determined by the behavior of free electrons. Therefore, the permittivity of a metal can be obtained from the response of free electrons to electromagnetic excitation. The starting point of the free-electron model is the electron equation of motion taking a decay caused by collisions with ions at rest into account by introducing a phenomenological decay constant. This model gives the dielectric function of a metal (the Drude free electron model)

$$\tilde{\varepsilon}(\omega)=1-\frac{4\pi Ne^2}{m_\mathrm{e}(\omega^2+\mathrm{i}\Gamma\omega)}=1-\frac{\omega_\mathrm{p}^2}{\omega^2+\mathrm{i}\Gamma\omega}\,, \tag{5}$$

where N is the electron concentration, Γ is the decay constant, and ω_p is the plasma frequency defined by

$$\omega_\mathrm{p}^2=\frac{4\pi Ne^2}{m_\mathrm{e}}\,. \tag{6}$$

The physical meaning of the plasma frequency is as follows. The permittivity $\tilde{\varepsilon}(\omega)$ in (5) is zero at the frequency equal to the plasma frequency. From the expression for the electric induction $\mathbf{D}$, we then obtain the polarization of the medium in the form

$$\mathbf{P}=-\frac{\mathbf{E}}{4\pi}\,, \tag{7}$$

which implies that a polarizing field exists in the medium. When free electrons are displaced in some direction, the Coulomb force, which appears due to the macroscopic displacement of electrons with respect to positive ions, attempts to return the electrons, and a collective oscillatory motion of electrons is induced, which is called volume plasma oscillations. Thus, volume plasmons are free oscillations (in the absence of an external field) of electrons in a metal, which are characterized by the frequency ω_p and a zero wave vector. These oscillations are longitudinal and cannot be excited by optical fields, which are transverse in nature. Such oscillations can be excited, for example, by an electron beam penetrating inside a material [8]. We note that volume plasmons in metals were first detected just under such excitation [9–11].

After the adoption of the concept of volume plasmons in metals, it became clear that surface plasmons are also possible in thin films [12, 13]. And while the energy of volume plasmons is $\hbar\omega_\mathrm{p}$, the energy of plasmons in films is $\hbar\omega_\mathrm{p}/\sqrt{2}$. Further spatial constraints on electron oscillations in metals lead to a new family of localized plasmons with the energy $\hbar\omega_\mathrm{p}/\sqrt{3}$.

The permittivity of a metal is a complex function and can be written in terms of its real and imaginary parts in the form [14]

$$\tilde{\varepsilon}(\omega)=1-\frac{\omega_\mathrm{p}^2}{\omega^2+\Gamma^2}+\mathrm{i}\,\frac{\omega_\mathrm{p}^2\Gamma}{\omega(\omega^2+\Gamma^2)}\equiv\varepsilon_1(\omega)+\mathrm{i}\varepsilon_2(\omega)\,. \tag{8}$$

The permittivity of a metal essentially depends on the frequency range under study. If the condition $\omega\gg\Gamma$ is satisfied, the permittivity is predominantly a real function

(absorption is insignificant) and the properties of the metal are close to those of a dielectric,

$$\tilde{\varepsilon}(\omega) \approx 1 - \frac{\omega_p^2}{\omega^2} . \quad (9)$$

When the condition $\omega < \omega_p$ is satisfied, the real part of the permittivity is close to zero (strong losses), and the metal substantially absorbs and reflects light. In the high-frequency range $\omega \gg \omega_p$, electrons in the metal have no time to follow the fast oscillations of the external field, and the metal absorbs weakly, and hence the permittivity again becomes a real function.

Despite its simplicity, the Drude model describes many optical properties of simple metals quite well. However, high-frequency interband transitions in real metals become substantial in the optical response of a metal and cause additional losses, which can be described by introducing an additional term ε_∞ to the equation for the permittivity,

$$\tilde{\varepsilon}(\omega) = \varepsilon_\infty - \frac{\omega_p^2}{\omega^2 + i\omega\Gamma} . \quad (10)$$

Typical values of ε_∞ lie in the range $1 \leqslant \varepsilon_\infty \leqslant 10$. We also note that plasmon oscillations in real metals appear not only at the frequency ω_p but also at other frequencies at which the permittivity vanishes.

2.1.2 Localization of plasmon oscillations. In isolated metal nanoparticles smaller than the penetration depth of an electromagnetic field in the metal, the external electromagnetic field causes the displacement of the whole free electron cloud with respect to lattice ions. Surface charges appearing on opposite sides of a nanoparticle create a recovering field producing oscillations of the electron cloud at frequencies determined by the electron density and the nanoparticle geometry. Such resonances were called *localized surface plasmon resonances* (LSPRs). Their excitation leads to an increase in the field amplitude both inside nanoparticles and near them (near-field amplification of the optical field). Localized surface plasmon resonances are nonpropagating excitations of conduction electrons in metal structures and, unlike propagating surface plasmon waves, can be excited by an external electromagnetic field. They usually have more than one oscillation mode. Different modes differ in the charge density and electromagnetic field distributions. The lowest-order field distribution is of the dipole type, whereas higher-order modes can be described by multipole charge distributions.

For nanoparticles smaller in size than the exciting field wavelength, the phase of the oscillating external field can be assumed constant over the particle size. In this case, the so-called electrodynamic quasistatic approximation is valid, in which the spatial field distribution can be calculated by solving a simplified problem for the behavior of a particle in a permanent electrostatic field E_0. The dielectric response of the nanoparticle is described by a complex dielectric function $\varepsilon_p(\omega)$, while the environment is assumed to be isotropic and described by a real permittivity ε_{out}. Inside a sphere, the external field E_0 induces a dipole moment proportional to the field strength

$$\boldsymbol{\mu}_{sph} = \varepsilon_{out}\alpha_{sph}(\omega)\mathbf{E}_0 , \quad (11)$$

where α_{sph} is the effective polarizability of the sphere of diameter R,

$$\alpha_{sph}(\omega) = R^3 \frac{\tilde{\varepsilon}_p(\omega) - \varepsilon_{out}}{\tilde{\varepsilon}_p(\omega) + 2\varepsilon_{out}} . \quad (12)$$

Elongated nanoparticles (such as nanorods) can be approximated in calculations by ellipsoids, because an exact solution of the Laplace equation exists in this case. The electric field inside an ellipsoidal nanoparticle is homogeneous but is no longer collinear to the applied external field [15]. The polarizability of the ellipsoid in the field parallel to one of its principal axes has the form [16]

$$\alpha_i(\omega) = 4\pi a_1 a_2 a_3 \frac{\tilde{\varepsilon}_p(\omega) - \varepsilon_{out}}{3\tilde{\varepsilon}_{out} + 3L_i\left(\tilde{\varepsilon}_p(\omega) - \varepsilon_{out}\right)} , \quad (13)$$

where L_i is the depolarization factor depending on the particle shape, and the subscript $i = 1, 2, 3$ denotes the polarization of the external field directed along one of the axes of the particle [16]. It is commonly accepted that the quasistatic approximation provides a good description of basic optical processes in metal nanoparticles smaller than 100 nm.

Field amplification. It follows from the expression for the polarizability of a spherical nanoparticle that for

$$\mathrm{Re}\left[\tilde{\varepsilon}_p(\omega)\right] \approx -2\varepsilon'_{out} , \quad (14)$$

the polarizability attains its maximum and the electromagnetic field is amplified. The mode in which this condition is satisfied is called the *dipole surface plasmon mode*. Condition (14) is satisfied for a negative permittivity. The resonance frequency in the free-electron Drude model is described by

$$\omega_{LSP} = \frac{\omega_p}{\sqrt{1 + 2\varepsilon_{out}}} . \quad (15)$$

It follows from (12) that the polarizability of a nanoparticle depends on the frequency and reaches its maximum for a spherical nanoparticle when the condition $\tilde{\varepsilon}_p(\omega) + 2\varepsilon_{out} = 0$ holds. In this case, the resonance amplification of the field occurs on its surface. It is common to consider amplification along the exciting field direction (parallel) and in the perpendicular direction as functions of the distance d to the surface:

$$A_\perp(\omega, d) = \left| 1 - \frac{\tilde{\varepsilon}_p(\omega) - \varepsilon_{out}}{\tilde{\varepsilon}_p(\omega) + 2\varepsilon_{out}} \frac{R^3}{(R+d)^3} \right| , \quad (16)$$

$$A_\parallel(\omega, d) = \left| 1 + 2\frac{\tilde{\varepsilon}_p(\omega) - \varepsilon_{out}}{\tilde{\varepsilon}_p(\omega) + 2\varepsilon_{out}} \frac{R^3}{(R+d)^3} \right| . \quad (17)$$

It follows from these expressions that on the surface of metal nanostructures a significant amplification occurs, whose magnitude depends on the losses in the metal.

2.1.3 Dependence of localized surface plasma resonances on the nanoparticle size and shape.

Particle size. The eigenfrequencies of localized plasmon resonances are determined by the size, shape, and material of nanoparticles [16]. The optical response of nanoparticles is determined by excitation of localized plasmon resonances of different orders [17, 18]. The type of collective oscillations essentially depends on the size of metal nanoparticles. For

small particles, these are collective electron oscillations. For large particles, the electron motion represents field-induced spherical plasmon polaritons. A distinctive feature of the two types of electron motions is the so-called 'hot' electron effect: the kinetic energy of individual electrons in large particles is negligible compared to the collective motion energy. The energy of individual electrons in small particles can be considerable, playing a key role in the optical properties of particles. 'Hot' electrons experience strong electron–electron scattering [19], resulting in breaking the phase coherence of collective motion.

In large nanoparticles, higher-order modes are excited. The solution of the Laplace equation with the corresponding boundary conditions shows the appearance of the effective multipole polarizability in a sphere [20],

$$\tilde{\alpha}_l(\omega) = R^{2l+1}\,\frac{\tilde{\varepsilon}_\mathrm{p}(\omega)-\varepsilon_\mathrm{out}}{\tilde{\varepsilon}_\mathrm{p}(\omega)+\big((l+1)/l\big)\varepsilon_\mathrm{out}}\,, \tag{18}$$

where the parameter l determines the multipole order: $l = 1$ is a dipole resonance, $l = 2$ is a quadrupole resonance, etc.

For large nanoparticles, the electric field of exciting radiation is no longer homogeneous on the particle scale because in this case $\lambda < d$. Because any external field can be expanded in multipoles, multipoles can be excited in a large nanoparticle. The contribution of the quadrupole term to the optical response of a nanoparticle already becomes noticeable for its size of about 30 nm. A quadrupole resonance in the Drude model appears at the frequency

$$\omega_\mathrm{LSP} = \frac{\omega_\mathrm{p}}{\sqrt{1+(3/2)\varepsilon_\mathrm{out}}}\,, \tag{19}$$

i.e., at a higher frequency than the dipole resonance does. The spectral response of the nanoparticle is still determined by its dipole resonance; however, as the nanoparticle size increases, contributions from multipole resonances become more pronounced. The resonance condition for higher-order resonances approaches the resonance condition $\varepsilon_\mathrm{p}(\omega) = -\varepsilon_\mathrm{out}$ for surface plasmon polaritons. In addition to the multipoles, *delay effects* also appear in large nanoparticles. One of the manifestations of this effect is the resonance frequency shift. Moreover, the radiative scattering by a nanoparticle becomes significant. It becomes quite noticeable for a nanoparticle radius of about 20 nm and dominates in extinction for radii above 100 nm.

The optical response of a nanoparticle can be determined by measuring its three main characteristics: *extinction, absorption,* and *scattering*. If a nanoparticle is placed into a light beam, a decrease in the beam light flux due to interaction with the nanoparticle is called the *extinction* of the incident light field. Extinction occurs due to light absorption and scattering. Absorption, scattering, and extinction depend on the nature of the nanoparticles, their size and shape, and the environment. These processes are quantitatively described by introducing the absorption cross section C_abs, the scattering cross section C_scat, and the extinction cross section C_ext, which are obviously related as

$$C_\mathrm{ext} = C_\mathrm{abs} + C_\mathrm{scat}\,. \tag{20}$$

For a spherical nanoparticle of a radius R much smaller than the light wavelength, expressions for absorption and scattering cross sections are determined from the corresponding polarizabilities and have the form [16, 19]

$$C_\mathrm{abs}(\omega) = \frac{4\pi\omega}{c}\,\mathrm{Im}\left[\tilde{\alpha}_\mathrm{sph}(\omega)\right] = 9k\,\frac{4\pi R^3}{3}\,\frac{\mathrm{Im}\left[\tilde{\varepsilon}_\mathrm{p}(\omega)\right]}{\left[\tilde{\varepsilon}_\mathrm{p}(\omega)+2\right]^2}\,, \tag{21}$$

$$C_\mathrm{scat}(\omega) = \frac{8\pi}{c}\,\frac{\omega^4}{3c^3}\,\left|\tilde{\alpha}_\mathrm{sph}(\omega)\right|^2 = \frac{8\pi k^4}{3}\,R^6\left|\frac{\tilde{\varepsilon}_\mathrm{p}(\omega)-1}{\tilde{\varepsilon}_\mathrm{p}(\omega)+2}\right|^2. \tag{22}$$

For small nanoparticles ($d < 30$ nm), absorption/extinction processes are mainly determined by the dipole plasmon resonance. In this case, scattering is negligible compared to absorption, because radiative processes require a coupling between electric and magnetic components of the field. Therefore, extinction is completely determined by absorption, while spectral characteristics are determined by the material characteristics of the nanoparticle medium and are independent of the nanoparticle geometry.

Because of the resonance frequency dependence of the absorption cross section, the light flux absorbed by small nanoparticles can be both higher and lower than the light flux incident on the area corresponding to the geometrical cross section of a nanoparticle. For example, an aluminum nanoparticle $kR = 0.3$ in size has an absorption cross section for 8.8 eV photons that is 18 times greater than its geometrical cross section. The absorption efficiency of the nanoparticle for 5 eV photons is only 0.1.

Shape of nanostructures. The optical and spectral properties of nanostructures greatly depend on the nanostructure shape. The nanostructure shape determines the intensity, number, and width of plasmon resonances. Their frequencies can be tuned in the spectral range from visible to near IR by changing their shape, size, and environment (Fig. 1). For nonspherical metal nanoparticles, an exact analytic solution for their response to an external electromagnetic field is absent in the general case. An ellipsoid is closest in shape to a sphere. For an ellipsoid much smaller in size than the light wavelength, the polarizability of the nanoparticle can be determined in the quasistatic approximation [16] [see (13)], which depends on the ellipsoid axes a_1, a_2, a_3, the permittivity of the nanoparticle metal, its environment, and a geometric factor L. For an ellipsoid, three plasmon resonances exist that are related to the possible directions of the light polarization vector along principal axes of the ellipsoid. The width, intensity, and position of resonances depend on the geometric factor L and the permittivities of the nanoparticle

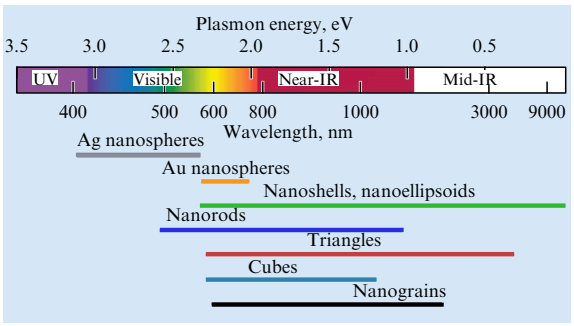

Figure 1. (Color online.) Spectrum of the localized surface plasmonic resonance of metal nanoparticles of various shapes. A plasmonic resonance is possible in a broad wavelength range, from UV to mid-IR for metal nanoparticles of various shapes and sizes [21]. © Nature Publishing Group. Reproduced by permission.

metal and its environment, and can be varied in a broad range.

A particular case of an ellipsoid is a spheroid in which two axes are identical. For a spheroid, two plasmon resonances, longitudinal and transverse, are observed at frequencies corresponding to oscillations of the electron cloud along the respective major and minor axes [22]. The longitudinal resonance in a spheroid is shifted to the red compared to a sphere of the same volume.

2.1.4 Spectral width of plasmon resonance modes. The width of plasmon resonances is determined by the material parameters of a nanoparticle (permittivity) and its geometry. The permittivity of not too small metal particles is quite well described by the permittivity of the bulk material, which can be represented as consisting of the interband part $\varepsilon = \varepsilon_\infty$ and the intraband part [expression (10)].

The behavior of quasi-free electrons changes due to their interaction with the surface and a break in the system periodicity. However, this effect is small for metal nanoparticles and can be taken into account as a correction to the decay constant [23]. The decay constant can be written as the sum of a constant γ_0 of the bulk material and an additional dimensional part γ_s [24]: $\gamma = \gamma_0 + \gamma_s$. The first term γ_0 is determined by the behavior of electrons in the bulk material [25], and the second term γ_s is inversely proportional to the nanoparticle diameter D, $\gamma_s = 2g_s(v_F/D)$, where v_F is the Fermi velocity and g_s is a constant close to unity. For nonspherical nanoparticles, a similar expression is valid with the diameter replaced by the effective electron localization size L_{eff}, depending on the dimensional parameters of the nanoparticle. Theoretical considerations for nonspherical nanoparticles show that the nonradiative term of the decay constant for LSPRs can be written as the sum of two terms, one of which is determined by the conduction band and the other by interband transitions.

Experiments have shown that the resonance considerably broadens and shifts with decreasing the nanoparticle size. This is essentially caused by the interaction of electrons with the surface. In the case of a free nanoparticle, the mirror (elastic) reflection of electrons from a pure surface is assumed. In this case, the electron momentum and (or) energy transfer in collisions with the surface is not expected, and therefore the dependence of the parameter γ on the nanoparticle size is not expected either. The contribution of the free surface to dissipation depends only on the number of mirror reflections from the surface. In this case, the dissipation of plasmon oscillations is completely determined by scattering on lattice phonons, impurities, and defects, as well as by the excitation of electron–hole pairs.

For nonfree nanoparticles, electron collisions can already be inelastic. Inelastic collisions depend significantly on the physical and chemical properties of the interface and determine the efficient electron energy dissipation in collisions of electrons with the interface [26].

For nonspherical nanoparticles, the influence of the surface on the resonance broadening is even more complicated. Optical spectra are usually characterized by introducing the reduced electron mean free path determining the effective electron localization length. The width of resonances in rod-shaped nanoparticles was properly explained in [27]. For particles of different shapes, predictions of the classical ballistic model and quantum mechanical calculations contradict each other [28].

We note that the frequency of resonances in nonspherical particles strongly depends on their shape, resulting in a large inhomogeneous broadening of resonances in studies of nanoparticle ensembles. Experimental investigations [29] with individual nanorods showed that longitudinal localized plasmon mode resonances can be described by three independent parameters: the central frequency Ω_R of the resonance, its width Γ, and area S. The extinction cross section of a nanorod is expressed in terms of these parameters as

$$\sigma_{ext}(\omega) = S\,\frac{\Gamma/2\pi}{(\omega-\Omega_R)^2 + (\Gamma/2)^2}\,. \qquad (23)$$

The spectral width Γ is determined by the radiative and nonradiative decay mechanisms for longitudinal localized plasmon oscillations with the corresponding widths Γ_r and Γ_{nr}. The nonradiative width Γ_{nr} is determined by absorption in the nanoparticle metal, and its value is related to the imaginary part of the permittivity.

As noted above, for a nanoparticle smaller in size than the skin layer, an external electromagnetic field penetrates through the entire nanoparticle, producing oscillations of all free electrons of the nanoparticle. Near the nanoparticle, a localized electromagnetic field arises that is stronger than the external field by a factor Q. Figure 2 shows the maximum field amplification on the surface of spherical nanoparticles made of gold, silver, titanium nitride, zirconium nitride, and transparent conducting oxides [30]. The increase in the field on the nanoparticle surface enhances its interaction with the environment of the nanoparticle. The absorption cross section of the nanoparticle greatly increases at resonance, achieving its maximum.

We can see from Fig. 2 that silver surpasses all other materials in light amplification in the blue spectral region. Other materials demonstrate comparable characteristics in some ranges in the visible and IR regions.

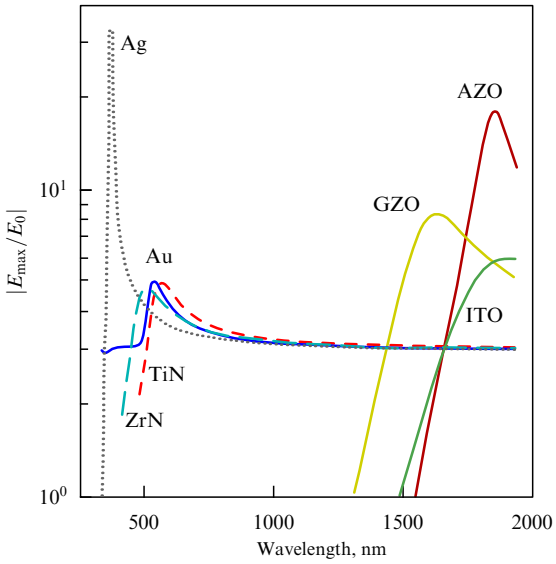

Figure 2. Maximum field amplification achieved on the surface of spherical particles made of gold, silver, titanium nitride, zirconium nitride, and transparent conducting oxides (GZO, AZO, ITO) [30] © Wiley-VCU Verlag GmbH & Co. KGaA. Used by permission.

2.1.5 Plasmon resonances of quantum-size particles. The properties of plasmon resonances of nanoparticles above 10 nm in size are very well studied [31]. For smaller sizes, when the quantum nature of the conduction electrons becomes significant, problems in the measurement of weak optical signals from nanoparticles appear. These problems relate to the detection of both absorption and scattering for the nanoparticles, because the efficiency of these processes decreases as the respective sixth and third power of the nanoparticle diameter [16].

One of the methods to theoretically describe the optical properties of such small nanoparticles is based on the Drude model with additional terms included into the bulk dielectric permittivity to take the electron scattering from the nanoparticle surface into account. This method predicts a small red shift of plasmon resonances, which, however, contradicts experimental results [32, 33].

A theoretical model [34] correctly describing the plasmon properties of quantum-size particles is based on a generalized free electron Drude model, taking contributions from three effects to the permittivity into account: these are interband transitions, electron collisions with the surface, and the quantum size effect. The quantum size of nanoparticles is taken into account for the electron cloud in an infinitely deep potential well on the physical boundaries of nanoparticles. For such particles, the energy levels in the conduction band become discrete and only certain electron and plasmonic transitions are allowed. The frequencies ω_{if} of these transitions correspond to the allowed transitions of conduction electrons between quantum energy levels, from the filled i states in the k space of the Fermi sphere to the unfilled f states immediately outside it [34].

Quantum-size particles are of interest not only from the general physical standpoint but also for practical applications because understanding plasmonic resonances of such particles is promising as regards their numerous uses in biology, catalysis, and quantum optics [35–37].

2.2 Nanostructure complementary to a nanoparticle: Babinet's principle

Babinet's principle is a classical concept of the wave theory of light [7]. This principle was originally used to simplify the analysis of some diffraction problems [38]. Babinet's principle in a scalar formulation establishes a correspondence between the diffraction field on some screen and the field on a so-called complementary screen. More rigorously formulated, Babinet's principle assumes that magnetic and electric fields are interchangeable for an ideally conducting planar structured screen and a screen 'complementary' to it [7]. Babinet's principle allows solving the problem of electromagnetic wave scattering in classical electrodynamics by replacing it with an equivalent problem for which the solution is known or can be found more easily.

Babinet's principle can be rigorously applied only to ideally conducting and infinitely thin metal screens. It has been successfully used for many years by the microwave community, mainly because the conductivity of most metals is high enough in the microwave frequency range and the wavelength greatly exceeds the characteristic size of structures. A simple example demonstrating the equivalence of the diffraction problem for complementary nanostructures is the problem of diffraction by a hole in an ideally conducting screen and the complementary problem of diffraction by an infinitely thin ideally conducting disc with the shape of the hole in the screen.

According to Babinet's principle, a group of metal nanoparticles and a complementary array of holes produce complementary optical spectra when irradiated with light with corresponding (mutually orthogonal) polarizations: the maximum transmission of the hole array is observed at the wavelength coinciding with the position of the extinction peak in the transmission of light through the group of complementary particles.

During the last decade, numerous metal nanostructures have become the subject of experimental and theoretical studies, including single nanoparticles, groups of metal nanoparticles [39, 40], and metal structured films [41, 42]. They are studied as building blocks of more complex structures in nanooptics and nanophotonics [43, 44]. The possibility of using Babinet's principle to create and study new metal nanoparticle constructions or thin metal nanostructured films is quite attractive. Babinet's principle has found wide applications, for example, in the design of metamaterials and nanoantennas in various spectral ranges, from visible to microwave [45, 46].

However, in the optical range, fundamental physical restrictions exist on the applicability of Babinet's principle. Boundary conditions for a metal are not strictly applicable because the field penetration depth is comparable to the structure size. In addition, nanostructures have relatively high losses in the optical range. The question arises as to the extent of applicability of Banbinet's principle to metal nanostructures in the *optical range*.

The optical response of nanostructures and complementary nanostructures can be studied in two regimes: in the far field (at distances from the nanostructure greatly exceeding the wavelength) and in the near field (at distances smaller than 100 nm). Far-field studies show that under certain conditions [upon complementary polarized excitation and the appropriate detection of reflection and transmission $|r(\Theta)|^2 \leftrightarrow T_c(\pi/2 - \Theta)$], Babinet's principle holds in the optical region, and complementary nanostructures have the same optical and spectral characteristics.

Near-field studies of complementary nanostructures show a difference in characteristics of nanostructures in the near zone. This is manifested, for example, in the study of SERS (surface-enhanced Raman scattering), which is largely determined just by the near-field electromagnetic field strength [47].

The use of Babinet's principle for predicting the response of metal plasma nanostructures much smaller in size than the light wavelength in the optical range does not always lead to conclusions consistent with experimental data. This is explained by a number of factors. For example, Babinet's principle is used for measuring the transmission through nanostructures, and the presence of resonance eigenmodes is ignored at the same time. The localized eigenmodes can make a considerable contribution to the optical properties of many nano- and microoptical devices such as subwavelength holes, optical antennas, or materials with new electromagnetic properties.

The situation becomes even more complicated in the study of nonlinear properties of metal nanostructures. For example, we consider the experimental study of second harmonic generation in two complementary nanostructures: magnetic split-ring resonators (SRRs) and complementary split-ring resonators (CSRRs) made in a metal nanofilm. An SRR is an

almost closed ring made of a metal wire, which can be treated as a subwavelength electromagnet in which the incident light field induces a circulating oscillatory electric current, which in turn results in the appearance of a localized magnetic field (a magnetic dipole moment perpendicular to the SRR plane). In the microwave spectral region, an SRR is the most popular resonance element for constructing metamaterials [48]. By decreasing the SRR size to a few nanometers, we can expect to obtain the eigenmodes of such a resonator in the optical range, as was demonstrated in [49–51].

Babinet's principle connecting the optical properties of complementary nanostructures is very useful for the design of metal nanostructures; however, it should be borne in mind that its is not universally applicable.

2.3 Optical properties of a single nanohole

A single subwavelength and nanometer hole in a conducting screen is a nanostructure complementary to a nanoparticle (nanodisc). The interaction of electromagnetic radiation with a subwavelength hole was first considered in the pioneering work by Bethe [52]. He studied the propagation of radiation through a subwavelength hole in an infinitely thin and ideally conducting screen and calculated the transmission cross section for the hole in the long-wavelength approximation ($a \ll \lambda$), which was later refined in [53] by taking higher-order terms into account:

$$\frac{\sigma}{\pi a^2} = \frac{64(ka)^4}{27\pi^2}\left[1 + \frac{22}{25}(ka)^2 + \ldots\right], \qquad (24)$$

where $k = 2\pi/\lambda$ and a is the hole radius. Expression (24) shows that the transmission cross section depends on the wavelength as $(a/\lambda)^4$. For $a < \lambda$, it rapidly decreases and for subwavelength holes becomes small compared to the geometrical cross section of the nanohole.

According to Babinet's principle, a nanosize hole in a conducting screen and a nanoparticle (nanodisc) can be characterized by the equivalent induced electric and (or) magnetic moments. Indeed, as shown in [52], the field at a large distance from the hole is equivalent to the field of two dipoles: a magnetic dipole parallel to the screen and an electric dipole perpendicular to the screen.

Numerical calculations in [54, 55] confirmed basic conclusions about the optical response of a nanohole and also showed that the scattering cross section is smaller than the geometrical cross section for the radii $a < 0.2\lambda$. In real metal screens, localized plasmon resonances can appear, which affect the value of the transmission cross section [56].

Considerable efforts were made to find a way to increase the transmission of radiation through a subwavelength hole. The possibility of increasing the light transmission through a nanohole compared to the Bethe theory prediction was first demonstrated for a *periodic array* of nanoholes [57, 58]. In the case of a *single* nanohole, light transmission can also be increased. This can be achieved by two methods. The first is based on using a material with a high permittivity ε inside the nanohole [59]. In this case, modes of the Fabry–Perot cavity type occur along the nanochannel due to the decrease in the effective radiation wavelength by a factor of $\sqrt{\varepsilon}$ inside the channel [60]. These modes are partially coupled to the continuum of light states outside the metal screen, which results in an increase in nanohole transmission. The width of resonances is determined by the strength of coupling of cavity modes to continuous-spectrum modes.

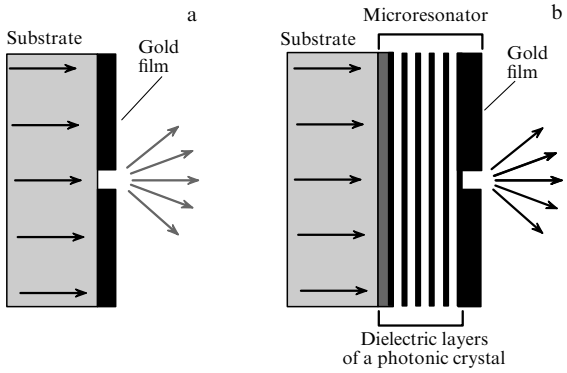

Figure 3. (a) Nanohole in a gold film deposited on a quartz substrate. (b) Nanohole in a gold film in a microresonator formed on a quartz substrate using a photonic crystal [62]. © MAIK NAUKA/INTERPERIODICA and Springer. Used by permission.

The second method for increasing the transmission of light through nanoholes involves creating a periodic corrugation on the surface around a nanohole [61]. The corrugation on the front surface of the screen (for example, using a periodic structure) provides efficient coupling of radiation incident on the screen to surface plasmons. By properly choosing the parameters of the optical system, one can achieve constructive interference between a plasmon surface wave and the wave passing through the nanochannel, which results in an increase in the field intensity inside the channel, thereby increasing the transmitted light. By making the corresponding corrugation on the rear surface of the screen, it is possible to realize the inverse process, providing a further increase in the transmission of light and its high directionality [61].

In [62–64], another mechanism for increasing the transmission of light through subwavelength nanoholes was proposed and realized. In this method, a nanohole is placed into the field of a mode of a one-dimensional photonic crystal (PC). Photonic crystals were proposed more than two decades ago [65]. One of the properties of PCs is the possibility of a strong spatial localization of the electromagnetic field [66]. This property makes PC-based micro- and nanoresonators very promising devices for studying quantum electrodynamics effects, because the Q factor of such resonators can reach high values (up to 10^6). The physical properties of a quantum mechanical system placed inside a PC resonator differ from those of the system in free space.

The authors of [62] proposed increasing light transmission thorough a nanohole (Fig. 3a) by placing the nanohole (an effective dipole) into the maximum field region of a one-dimensional PC (Fig. 3b). This creates conditions under which the re-emission rate of the effective dipole increases, resulting in an increase in the radiation power transmitted through the nanohole.

A microresonator (Fig. 3b) is made of a one-dimensional PC formed by alternating dielectric layers with the same optical thickness $h = \lambda/(4n)$, where λ is the light wavelength and n is the refractive index of the material of the layers. Dielectric layers are arranged such that a layer with a high refractive index is followed by a layer with a low refractive index [62]. Dielectric layers form a one-dimensional PC weakly transmitting light in the spectral range that is the forbidden band of the PC. A microresonator is built by depositing a gold layer on dielectric layers (Fig. 3b). The

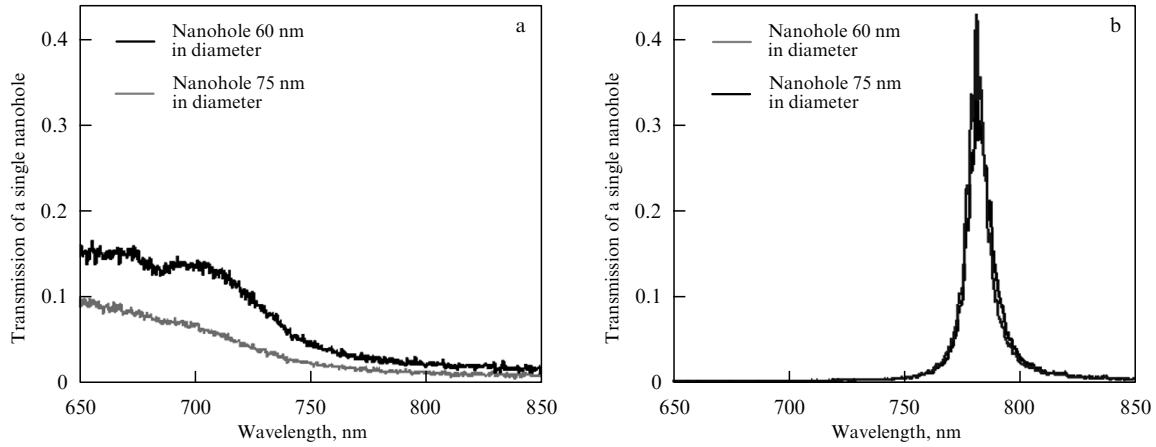

Figure 4. Transmission spectra of nanoholes of various diameters in (a) a reference gold film and (b) a gold film in a microresonator [63]. © MAIK NAUKA/INTERPERIODICA and Springer. Used by permission.

Q factor of the microresonator is about 100, this value being determined by absorption in gold.

The microresonator results in the formation of a narrow spectral mode inside the forbidden band of the PC. In the experiments in [62, 63], the mode resonance appeared at the wavelength $\lambda_{\rm res} = 792$ nm. The width of the resonance was 8.8 nm, corresponding to the microresonator factor $Q = \omega/\Delta\omega \approx 90$. Despite the moderate Q factor of the microresonator, this microresonator configuration has the important property of the *considerable amplification of the light field near the gold film surface*.

Measurements of the transmission through the holes 60 nm in diameter in a control gold film showed that the increase in the nanohole transmission upon increasing its diameter is in good agreement with the Bethe theory. For nanoholes in the microresonator, the dependence of the nanohole transmission on its diameter is no longer described by the Bethe theory, being determined by the following processes: (i) the light field amplification in the microresonator, (ii) the propagation of light through the nanohole, (iii) the change in the characteristics of the resonance mode of the microresonator due to the presence of the nanohole, and (iv) the influence of the microresonator on the propagation of light through the nanohole.

The transmission of a single nanohole 60 nm in diameter achieved in a microresonator in [63] was $T_1 \approx 41\%$ (Fig. 4), whereas the transmission in a control gold film was only $T_1 \approx 1.5\%$. Thus, the use of a microresonator provided the high spectral selectivity of light transmission through a single nanohole.

2.4 Thermal phenomena at the nanoscale: nanoparticles vs nano-openings

Physical laws used in simulations of macroscopic systems are typically invalid when the system size approaches the spatial characteristics of the physical problem, such as the mean free path of carriers. In this case, the physical description of systems has to be modified. This general statement is also valid for a description of thermal phenomena in microsize systems and even more so for nanosize systems.

The heat transfer phenomenology is significantly different at the macro- and microspatial scales. While the heat transfer at macroscopic scales is considered a slow process (for example, the heat conduction time scale in macroscopic systems about 1 m in size is a few minutes), the heat transfer at the microscopic level is an extremely fast and efficient process at the time scale of ~ 10 ns. The heat transfer at the microscale is virtually inertialess. This statement is all the more valid for heat transfer at the nanometer scale.

The heat conduction in a homogeneous medium is described by the diffusion equation [67]

$$\rho c_{\rm p} \frac{\partial T}{\partial t} = k\nabla^2 T, \tag{25}$$

which, with the expression $a = k/\rho c_{\rm p}$ for the heat conductivity, takes the form

$$\nabla^2 T = \frac{1}{a}\frac{\partial T}{\partial t}. \tag{26}$$

The heat conduction equation in the dimensionless form after the change of variables $t = t^+ t_0$ and $x = x^+ L$ becomes

$$\nabla_+^2 T = \frac{L^2}{at_0}\frac{\partial T}{\partial t^+}, \tag{27}$$

where t_0 and L are the characteristic temporal and spatial size of the problem. It follows from Eqn (27) that the problem of thermal field formation depends only on the dimensionless quantity at_0/L^2, known as the Fourier number. To visualize the typical behavior of the diffusion phenomenon, the behavior of the system is considered under the action of temporal and spatial delta pulses:

$$\nabla^2 T - \frac{1}{a}\frac{\partial T}{\partial t} = S\delta(t)\delta(r). \tag{28}$$

Equation (28) describes the temperature field distribution produced by a thermal pulse at the space–time point $r = 0$, $t = 0$. The solution of Eqn (28) has the form

$$T(r,t) = \frac{S}{(4\pi at)^{3/2}} \exp\left(-\frac{r^2}{4at}\right). \tag{29}$$

This solution describes a Gaussian spatial energy distribution with the characteristic width $2\sqrt{at}$. After some time t, the thermal energy fills the volume of a sphere with the

radius $2\sqrt{at}$. When a body of radius R is heated by absorbing energy on its surface, the time required for its thermalization is determined by the heat diffusion time through its volume: $t_{cd} \sim R^2/a$. For a sphere 1 cm in diameter, this time is of the order of 100 s. For a nanosphere 100 nm in diameter, this time decreases by many orders of magnitude, to 10 ns. For a sphere 1 nm in diameter, the thermalization time is estimated as ~ 1 ps. However, the considerations presented above are, strictly speaking, no longer valid at the nanometer spatial scale. We have reached the limit of applicability of macroscopic heat transfer models. Another characteristic time of the physical problem becomes relevant: the phonon relaxation time, which lies in the picosecond range. Therefore, the diffusion equation should be changed. This problem appears because the Fourier law describes an instant response to an external excitation. We described the system on the nanoscale by neglecting its response time determined by microscopic collision processes.

Another physical limitation appears when the geometrical dimensions of the system become comparable to the phonon wavelength. In this situation, quantization effects already become essential, and this can lead to the heat-conduction quantization [68], similar to what is well known for the electric conduction [69].

Resonance metal nanoparticles absorb radiation very efficiently. As mentioned above, the absorption cross section of a nanoparticle at the resonance frequency can greatly exceed its geometrical cross section. The scattering cross section of a metal nanoparticle also increases at the resonance frequency. Depending on the nanoparticle size, either scattering or absorption can dominate. For small nanoparticles (less than 15 nm), absorption exceeds scattering. As the nanoparticle size is increased, scattering begins to exceed absorption. Therefore, metal nanoparticles are very inefficient fluorophores, with the quantum yield of fluorescence of about 10^{-5} or lower. Almost all light incident on a nanoparticle is absorbed and transformed into heat, and the nanoparticle can be treated as an efficient heat generator on the nanometer scale [70, 71]. Because the resonance frequencies of nanoparticles can be tuned to a certain wavelength (by choosing their material, topology, and environment) in a broad frequency range from the visible to IR range, the transformation of laser radiation into heat is also frequency selective.

The important characteristics of laser radiation absorption by a nanoparticle are the nanoparticle temperature after absorption and the time and spatial dependences of the nanoparticle and its environment temperature. These parameters essentially depend on the particle illumination regime, either continuous or pulsed. A typical experimental situation in which a metal nanoparticle is heated (intentionally or undesirably) appears under irradiation of the nanoparticle by laser light. The heat dissipation after light excitation occurs due to fast dephasing of the coherent electron motion in conjunction with the fast energy transfer to the metal crystal lattice. The heat is generated very rapidly and thermalization develops for a time of the order of a few picoseconds. On the other hand, the environment temperature increases for considerably longer times determined by physical heat conduction processes.

If the nanoparticle size is much smaller than the wavelength, the optical response of the nanoparticle is described sufficiently well by an electromagnetic dipole with the polarizability determined by expression (12). The optical response efficiency (scattering and absorption) is characterized by the corresponding absorption and scattering cross sections [16]

$$\sigma_{abs} = k\,\mathrm{Im}\,(\alpha) - \frac{k^4}{6\pi}\,|\alpha|^2\,, \tag{30}$$

$$\sigma_{scat} = \frac{k^4}{6\pi}\,|\alpha|^2\,, \tag{31}$$

$$\sigma_{ext} = \sigma_{abs} + \sigma_{scat} = k\,\mathrm{Im}\,(\alpha)\,. \tag{32}$$

The power absorbed by the nanoparticle is expressed in terms of the absorption cross section σ_{abs} as $Q = \sigma_{abs} I$, where I is the radiation intensity incident on the nanoparticle. For a plane wave, the radiation intensity is related to the field strength as $I = n_s c_0 \varepsilon_0 |E_0|^2/2$. The power absorbed by the nanoparticle can also be obtained from the thermal energy density $q(\mathbf{r})$ inside the nanoparticle, while the generated heat is directly proportional to the electric field squared *inside* the metal [72].

Nanoparticles can be illuminated by either continuous laser radiation or laser pulses.

Continuous illumination regime. The stationary temperature distribution $T(\mathbf{r})$ inside and outside a nanoparticle can be found by solving the heat diffusion equation. In the stationary regime, the heat diffusion equation has the form [73]

$$\nabla \cdot \left[\kappa(\mathbf{r})\nabla T(\mathbf{r})\right] = -q(\mathbf{r})\,, \tag{33}$$

where q is the power density of an external heat source and $\kappa(\mathbf{r})$ is the heat conductivity. Outside the nanoparticle, $q = 0$. For a spherical nanoparticle of radius R, the increase in temperature is determined by the equation [74]

$$\delta T_{NP} = \frac{Q}{4\pi\kappa_S R}\,. \tag{34}$$

The spatial temperature distributions inside and outside a nanoparticle are [74]

$$\delta T(r) = \delta T_{NP}\,\frac{R}{r}\,, \quad r > R\,, \tag{35}$$

$$\delta T(r) \approx \delta T_{NP}\,, \qquad r < R\,. \tag{36}$$

As mentioned above, the stationary temperature regime is achieved very rapidly. The duration τ_{tr} of the transient regime is independent of the temperature increase but is determined by the characteristic size L of the system [75],

$$\tau_{tr} \sim L^2\,\frac{\rho c_p}{3\kappa_S}\,, \tag{37}$$

where ρ is the nanoparticle material density and c_p is its specific heat at constant pressure. For example, for spherical nanoparticles 10 nm, 100 nm, and 1 μm in diameter, we obtain respective durations τ_{tr} of about 0.1 ns, 10 ns, and 1 μs from (37). For nonspherical nanoparticles, a simple analytic expression describing the increase in the temperature as a function of the absorbed energy is absent, and the process has to be simulated numerically.

Pulsed illumination regime. Pulsed illumination of a nanoparticle gives rise to additional effects: (i) a fast change

in temperature and pressure, (ii) pronounced temperature-field localization [75], (iii) modification of the topology of the nanoparticles and nanostructures [31], and (iv) their possible melting. In this regime, the absorption of the laser pulse energy by a metal nanoparticle can be described as a three-stage process [76, 77].

The first stage is the absorption of radiation by electrons. At this stage of the interaction of a nanoparticle with a laser pulse, a part of the incident pulse energy is absorbed by the gas of free electrons of the nanoparticle. The electron gas is thermalized in a very short time (~ 100 fs) to the Fermi–Dirac distribution with the characteristic electron temperature T_e [76, 77]. This leads to a nonequilibrium thermal state in the nanoparticle because the lattice temperature T_p does not change over that times.

At the second stage, electron–phonon thermalization occurs. During this process, the hot electron gas is cooled due to electron–phonon interaction for the time τ_{e-ph}, and then the temperatures of the electron and ion subsystems of the nanoparticle material equalize ($T_e = T_p$). The characteristic times of this stage are independent of the nanoparticle size down to sizes lower than 5 nm [78]. For large particles and moderate pulse energies, the time scale of this process is $\tau_{e-ph} \sim 1.7$ ps [79].

At the third stage, heat diffuses to the nanoparticle environment. The heat diffusion from a nanoparticle to the environment typically occurs at longer time scales τ_{tr} [Eqn (37)] and leads to the nanoparticle cooling and the environment heating. The time scale of this process depends on the nanoparticle size and lies in the range from 100 ps to a few nanoseconds. For small nanoparticles (< 20 nm), the third stage can partially coincide in time with the electron–phonon thermalization stage [80].

The laser pulse duration compared to the time τ_{tr} determines variants of the possible development of the three-stage process. For a very short pulse (< 0.1 ns) and (or) a small enough nanoparticle (< 100 nm), we can assume that the three processes occur successively. In this regime, the nanoparticle temperature is determined by the laser pulse energy density F, the absorption cross section σ_{abs}, and the nanoparticle volume V and its material characteristics (the density ρ_{met} and the heat capacity c_{met} of a metal). The temperature reaches the maximum value equal to [75]

$$\delta T_{NP}^0 = \frac{\sigma_{abs} F}{V \rho_{Au} c_{Au}} . \tag{38}$$

In this case, the medium heating duration is of the order of τ_{tr}.

If the pulse duration exceeds τ_{tr}, the three processes overlap in time. In other words, heat is absorbed and supplied to the environment simultaneously. In this case, the maximum increase in temperature inside a nanoparticle does not reach δT_{NP}^0 and the heating duration is equal to the pulse duration. Such a situation occurs for a laser pulse duration of about a nanosecond.

Another important aspect of nanoparticle heating is the spatial temperature distribution in the nanoparticle vicinity. While the temperature profile changes by the $1/r$ law under continuous illumination, pulsed excitation allows additionally restricting the spatial distribution of the temperature field near a nanoparticle. For example, for a spherical nanoparticle of radius R, the temperature profile changes as $1/r^3$ for $r \ll R$. At the same time, it can be approximated by an exponential dependence in the vicinity of a nanoparticle (for $r \sim R$) [75]:

$$F(r) = \exp\left[-\left(\frac{r-1}{r}\right)^n\right], \tag{39}$$

where n is a fitting parameter.

The optical heating of a metal nanoparticle has two basic features: (i) the heating is strongly spatially localized in the vicinity of nanoparticle with a characteristic size in the range from a few tens to hundreds of nanometers and (ii) the heating occurs very rapidly and the maximum temperature is achieved in less than 50 ns. For such high laser energy absorption rates (with the pulse duration from nanoseconds to femtoseconds), the nanoparticle accumulates a great amount of heat and can melt [81]. If the nanoparticle is located on a surface, it can be ablated from the surface without melting [82].

The geometry of the nanoparticle and its environment strongly affect the heating [83]. Under irradiation of a nanostructure by laser pulses, the thermal destruction of a metal *nanostructure* occurs at lower laser radiation intensities than in the Babinet-*complementary structure* prepared in a metal film. Figure 5 illustrates this significant difference: Fig. 5a shows the temperature distribution calculated for an aluminum *nanorod* 50×570 nm^2 in size, and Fig. 5b shows a similar distribution for a *nanoslit* of the same size made in an aluminum film 50 nm in thickness. Both structures are illuminated by a monochromatic plane wave at 1560 nm with the power density 8×10^{13} W cm^{-2}. The polarization of radiation for the nanorode is directed along its axis, while for the nanoslit it is perpendicular to the longer side of the nanoslit, and hence the resonance excitation of plasmon oscillations occurs in both cases. Figure 5 shows that the nanorod is heated to considerably higher temperatures (by more than an order of magnitude) than is the nanoslit irradiated by the same laser power.

3. Optical nonlinearity of a single plasmonic nanostructure

3.1 Nonlinear properties of a single plasmonic nanostructure

The universally adopted description of nonlinear optical phenomena uses the concept of polarization $P(t)$ induced in a medium (nanostructure) by an external electromagnetic field $E(t)$ [84]. The polarization plays a key role in the description of nonlinear optics phenomena because its change in time is a source of new components of the electromagnetic field. The wave equation in a nonlinear optical medium takes the form [84]

$$\nabla^2 E - \frac{n^2}{c^2}\frac{\partial^2 E}{\partial t^2} = \frac{1}{\varepsilon_0 c^2}\frac{\partial^2 P_{NL}}{\partial t^2} , \tag{40}$$

where n is the linear refraction coefficient and c is the speed of light in a vacuum. The polarization $P(t)$ induced in the medium can be expanded in a power series in the field strength $E(t)$:

$$\begin{aligned} P(t) &= \varepsilon_0\left[\chi^{(1)}E(t) + \chi^{(2)}E^2(t) + \chi^{(3)}E^3(t) + \ldots\right] \\ &\equiv P^{(1)}(t) + P^{(2)}(t) + P^{(3)}(t) + \ldots . \end{aligned} \tag{41}$$

Here, $\chi^{(2)}$ and $\chi^{(3)}$ are the second- and third-order nonlinear optical susceptibilities, and the expansion terms $P^{(2)}(t) =$

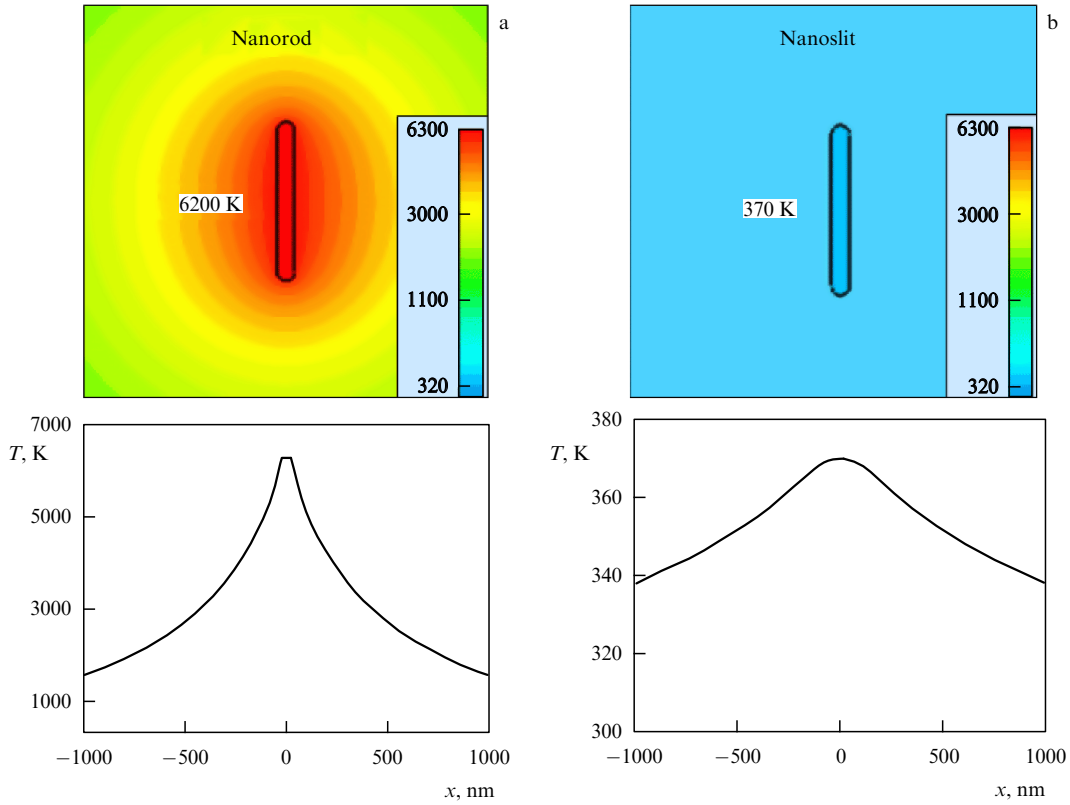

Figure 5. (Color online.) Calculated two-dimensional spatial temperature distribution and its one-dimensional cross section in nanostructures: (a) aluminum nanorod $50 \times 50 \times 570$ nm^3 in size; (b) nanoslit 50×570 nm^2 in size in a 50 nm thick aluminum film [83]. © IOP Publishing. Used by permission.

$\varepsilon_0\chi^{(2)}E^2(t)$ and $P^{(3)}(t) = \varepsilon_0\chi^{(3)}E^3(t)$ are the second- and third-order nonlinear polarizations.

The nonlinear optics of metals comprises the optics of surfaces, nanostructured surfaces, and nanostructures, because radiation penetrates into a metal only to a depth of the order of a skin layer. From the physical standpoint, optical nonlinearity appears in metal nanostructures due to the motion of electrons in strong laser fields. The motion of free electrons in plasmonic nanostructures in strong laser fields is characterized by large oscillation amplitudes. This leads to the anharmonicity of the electron *cloud* motion, resulting in the appearance of an effective nonlinear dipole moment [85]. The known effects of nonlinear optical interaction of laser radiation with nanostructures are the generation of harmonics [86–91] and parametric frequency summation [92–94]. Examples of the manifestation of the *single*-electron dynamics in plasmonic nanostructures are one-photon [95–97] and multiphoton luminescence [98–101].

By controlling the geometry of nanostructures, it is possible to vary the type of their nonlinear optical interaction with laser radiation [102, 103]. The interaction of laser radiation with nanostructures with a 'smooth' surface is mainly characterized by the coherent dynamics of an *ensemble* of free electrons (plasmons). This interaction leads to the generation of radiation harmonics. A fundamentally different scenario is realized when variations with the characteristic size of about 10 nm are produced on the nanostructure surface, which can lead to the domination of the *single*-electron dynamics, and nonlinear optical interaction is manifested as multiphoton luminescence.

3.2 Second-harmonic generation from a nanohole

One of the best known and widely used results of the appearance of second-order polarization under the action of an external field is the second-harmonic generation. The second-harmonic frequency 2ω generated by the exciting field at a frequency ω is determined by the second-order polarization

$$P_i(\omega_3) = \varepsilon_0 \sum_{jk} \chi^{(2)}_{ijk}(\omega_3, \omega_2, \omega_1)\, E_j(\omega_2) E_k(\omega_1) \qquad (42)$$

induced in the medium. The symmetry properties of the optical medium impose restrictions on the linear and nonlinear susceptibility tensors. For example, for a centrally symmetric optical medium, the nonlinear susceptibility $\chi^{(2)}$ must be identically zero. On the other hand, third-order nonlinear optical interactions can be realized in both centrally symmetric and not centrally symmetric media.

Second-harmonic generation is a process forbidden for centrally symmetric materials. Passing from a bulk material to the material surface removes the inversion-symmetry condition, thereby allowing second-harmonic generation on the surface of a material with any symmetry group. Nonlinear quadratic effects on metal surfaces, where the central-symmetry condition is broken, have been known for many decades [104].

The surface morphology also affects the efficiency of second-harmonic generation on a surface. Modern nanolithographic methods allow creating the desired surface morphology and considerably amplifying optical fields, thereby providing efficient second-harmonic generation [105].

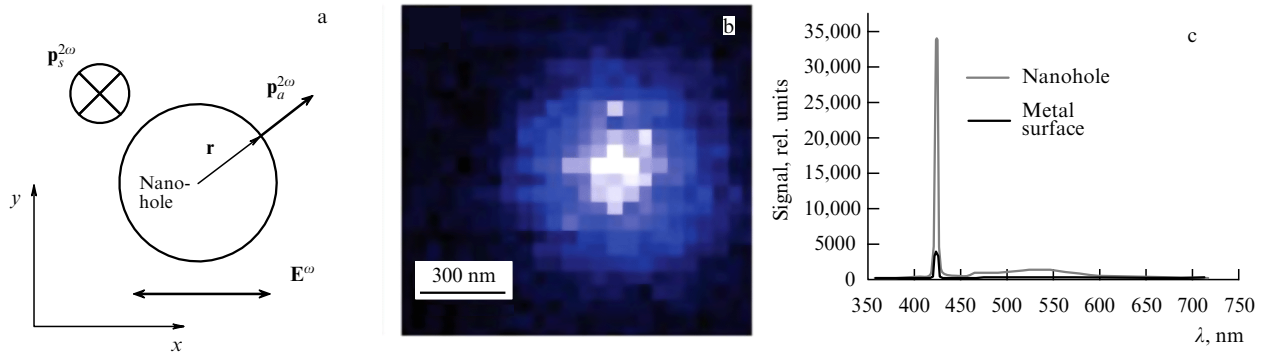

Figure 6. (a) Nonlinearly induced dipoles in a nanohole in a metal film, (b) nanoaperture image at the second-harmonic wavelength representing a diffraction-limited subwave spot, (c) emission spectrum from a nanoaperture in a metal surface [109]. © OSA. Used by permission.

The record value of the second-harmonic generation efficiency for nanoparticles is $\sim 10^{-7}$ [102, 106]. Adding dielectric nanostructures with high optical nonlinearity near plasmonic nanostructures can increase this efficiency by a few times [106]. In addition, the presence of interband transitions at the harmonic wavelength can also significantly increase the harmonic generation efficiency [94]. Although the achieved efficiencies seem extremely low, the harmonic generation efficiency reduced to the nanostructure volume has a record high value, which is more than six orders of magnitude higher than these efficiencies for nonlinear materials such as $LiIO_3$, KDP, KTP, and $LiNbO_3$, widely used in optics [107].

Two approaches to the study of the nonlinear optical interaction of light with a nanostructure are known. The first uses a nanoparticle as a nanostructure. The other approach uses a complementary nanostructure, nanoholes. The use of nanoparticles leads to a number of significant restrictions such as (i) the presence of the accompanying exciting radiation background at the excitation frequency and (ii) as mentioned above, the possible destruction of nanostructures at high laser radiation powers. A nanohole made in a metal surface allows using high laser radiation intensities without surface destruction, and at the same time a nanohole in the metal surface provides a considerable enhancement of the optical field in a nanovolume near the hole [108]. A nanohole in a metal screen offers a number of advantages over a nanoparticle for applications in nanoplasmonics, especially in nonlinear nanoplasmonics [102, 103]. They include (i) a weak exciting radiation background, greatly reduced by the weak transmission of the nanohole and (ii) stability against high-intensity radiation provided by the efficient heat removal by the metal film in which the nanohole is made [83].

The optical properties of a nanohole in a metal surface can be considered in terms of the properties of a nanostructured surface. A different approach uses Babinet's principle. According to this principle, the optical properties of a nanohole in a metal can be directly related to the properties of a metal nanodisc (of the size of the nanohole) [38].

The efficient second-harmonic generation from a single hole made in a 200 nm thick gold nanofilm with nanoholes 125–425 nm in diameter was demonstrated in [109]. The studies were performed using a tunable 150 fs, 850 nm, and 80 MHz femtosecond laser. The second-harmonic generation from nanoholes was observed at a wavelength of 425 nm (Fig. 6c).

The second-harmonic generation from a nanohole can be simulated using a nonlinear tensor with the largest diagonal coefficient $\chi^{(2)}_{nnn}$ (n is the direction to the metal–air interface) and smaller nondiagonal coefficients $(\chi^{(2)}_{ntt}, \chi^{(2)}_{tnt}, \chi^{(2)}_{ttn})$ [110]. For a nanohole (Fig. 6a), the components $p_i^{2\omega} = \sum_{jk} \chi^{(2)}_{ijk} E_j^{\omega} E_k^{\omega}$ of a nonlinear dipole responsible for the harmonic generation determine generation from two regions: (i) the edge of the nanohole aperture and (ii) the illuminated metal film surface around the hole. Calculations in [111, 112] show that the contribution from the hole edge is an order of magnitude higher than from the surface. For a nanohole 220 nm in diameter, the second-harmonic enhancement factor with respect to the metal surface was about 2, although the structure is centrally symmetric. The larger enhancement factor is expected for a nanohole with a different shape, which was confirmed for triangular holes, which are not centrally symmetric [109, 113].

Figure 6b shows an optical microscope image of a nanohole at the second-harmonic wavelength, which is a diffraction-limited subwavelength spot. The emission spectrum of such a nanohole contains the dominating second-harmonic signal and the shifted two-photon luminescence spectrum (Fig. 6c) related to interband transitions in gold.

3.3 Third-harmonic generation from a nanohole

Third-order nonlinear optical processes are determined by the following term of the induced nonlinear polarization:

$$P^{(3)}(t) = \varepsilon_0 \chi^{(3)} E^3(t)\,. \tag{43}$$

If excitation is produced by a monochromatic light wave $\tilde{E}(t) = E\cos(\omega t)$, the induced polarization can be written as

$$P^{(3)}(t) = \frac{1}{4}\,\varepsilon_0 \chi^{(3)} E^3 \cos(3\omega t) + \frac{3}{4}\,\varepsilon_0 \chi^{(3)} E^3 \cos(\omega t)\,. \tag{44}$$

The first term in the right-hand side of (44) describes the response of the system at the frequency 3ω and is responsible for the third-harmonic generation. The second term describes the nonlinear contribution to polarizatioin at the incident field frequency and is responsible for the nonlinear contribution to the refractive index at the frequency ω.

By now, numerous investigations have been performed in nanoplasmonics on the third-harmonic generation from metal surfaces [114–118], metal nanostructured

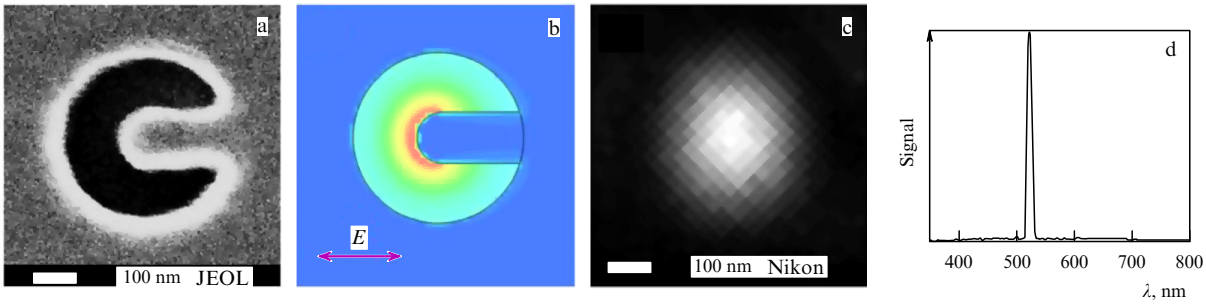

Figure 7. (Color online.) Third-harmonic generation from an SHR nanostructure made in a 50 nm thick aluminum film: (a) electron microscope image of a nanostructure, (b) calculated field distribution under illumination of the nanostructure by a 1560 nm monochromatic plane wave, (c) optical image of a nanostructure excited by a 1560 nm laser line and detected at the 520 nm third-harmonic wavelength, (d) measured third-harmonic spectrum. The radiation polarization is directed along the nanorod forming the nanostructure [102]. © OSA. Used by permission.

surfaces [114, 116, 119, 120], nanoparticle ensembles [51, 103, 121–123], and single nanostructures [18, 102, 124, 125]. Metal nanostructures have been studied in the form of nanorods (nanoantennas) [106, 124] and nanoholes [18, 126]. The efficiency of nonlinear processes highly depends on the shape and size of the nanostructures. For example, the efficiency of a circular nanohole is a few orders of magnitude lower than that of a nanorod [127] or a nanoslit [83, 126]. The difference is due to the great difference in the field enhancement near nanostructures.

Efficient third-harmonic generation was achieved using a hybrid nanostructure proposed in [102]. This nanostructure combines the advantages of nanorods (strong nonlinear properties) and nanoholes in a metal screen (the absence of background radiation and high radiative stability). Figure 7a shows the geometry of such a nanostructure, representing a nanohole made in a metal film with a nanorod located inside the nanohole. This nanostructure was called a spin-hole resonator (SHR) [102].

Calculations showed that the radiation conversion efficiency in the SHR nanostructure significantly depends on its geometry (the nanostructure diameter and rod length), the film material, and the refractive index of the environment. This is explained by the strong dependence of the excitation efficiency of localized plasmons on the nanostructure geometry and its local environment [58], which determine the distribution and amplitude of the electromagnetic field near the nanostructure. Third-harmonic generation greatly depends on the nanohole diameter and the nanorod length. The resonance behavior of the SHR nanostructure is interpreted as follows [102]. A plasmonic wave propagates in the nanostructure along its perimeter, the metal–dielectric interface. The reflection of the plasmon wave from the nanorod of the SHR nanostructure is equivalent to reflection from a mirror. As a result, if the length of the nanostructure-hole perimeter is equal to an integer number of the half-waves of the plasmon wave, Fabry–Perot resonances are excited in the nanostructure. The length of the nanorod in the SHR nanostructure determines the reflection coefficient and phase shift of the plasmon wave.

Figure 7b shows the calculated field distribution in an SHR nanostructure irradiated by a 1.5 μm plane wave corresponding to the plasmonic resonance of the nanostructure. The spatial distribution of the field shows that such a nanostructure forms a one-pole antenna, with the field localized near the end of the rod. An important property of the SHR nanostructure is the strong dependence of the resonance frequencies of its plasmonic oscillations and therefore its optical properties on the nanostructure size and shape. To create nanostructures with specified optical properties, their geometry should be controlled with an accuracy of the order of $\lambda/10$. As shown in [102], in the nonlinear optics of a single nanostructure, it is necessary to control its geometry with an even higher accuracy, of the order of $\lambda/100$. Such a high accuracy is required in order to control the surface electron states specified by irregularities on the nanostructure surface.

The third-harmonic generation with an SHR nanostructure was studied experimentally in [102] (Figs 7b, c). Nanostructures were made in a 50 nm thick aluminum film using a focused ion beam and were irradiated by 120 fs, 1560 nm, and 15 mW laser pulses focused on a spot 4.5 μm in diameter. The film material chosen had strongly nonlinear optical properties: the optical nonlinearity coefficient $\chi^{(3)}$ of aluminum at a wavelength of 1560 nm is approximately three orders of magnitude higher than that of gold [83]. The choice of the radiation wavelength is related to its use in modern telecommunications.

Another important property of the SHR nanostructure is a strong dependence of its nonlinear optical response on the incident radiation polarization. Figure 8 shows the dependence of the third-harmonic intensity on the exciting radiation polarization. The figure shows that the third-harmonic generation efficiency is minimal when the radiation polarization is orthogonal to the nanorod. For radiation polarization turned by 90°, the third-harmonic radiation power increases by a factor of 40,000. The high sensitivity to polarization is explained by the cubic dependence of the third-harmonic generation efficiency on the incident radiation intensity. We note that the polarization dependence of the third-harmonic generation in SHR nanostructures is as efficient as that of a Glan prism, one of the best polarization optical elements.

Third-harmonic generation in the UV spectral range. Of special practical interest is the harmonic generation in nanostructures in the UV range. First, this allows the creation of nanolocalized UV radiation sources required for nanodiagnostics and nanolithography. Second, the high optical nonlinearity of nanoparticles in the UV spectral range can be used in cell phototherapy [129].

The generation of UV radiation by plasmonic nanostructures has been poorly studied. There are only a few experimental studies [130, 131] demonstrating the third-harmonic generation in nanostructures excited by a femtose-

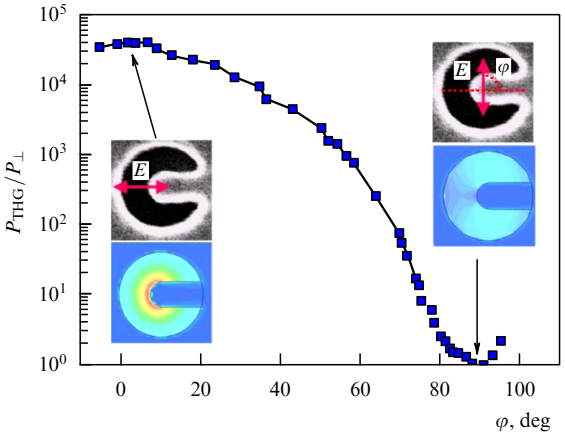

Figure 8. (Color online.) Dependence of the third-harmonic amplitude on the exciting light polarization. Insets show the calculated near-field distributions at the fundamental frequency for the maximum and minimum third-harmonic generation effects [128]. © OSA. Used by permission.

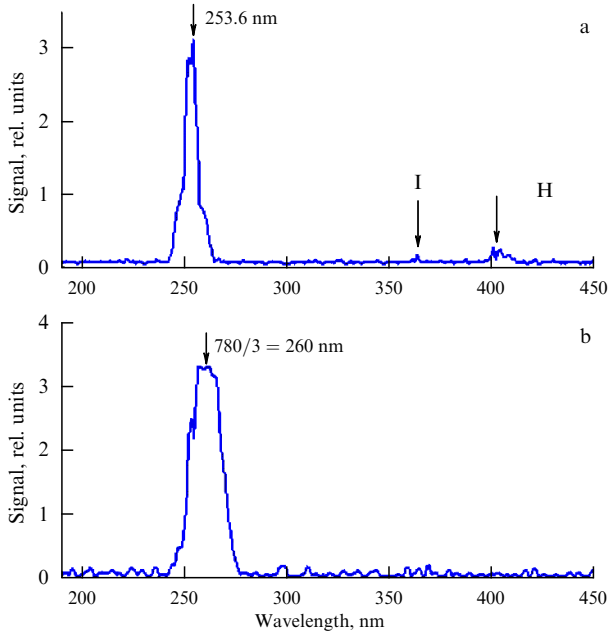

Figure 9. Third-harmonic generation in the UV range from a nanoslit in a metal film: (a) emission spectrum of a mercury lamp transmitted through a 150 nm nanohole in a 200 nm thick gold film, (b) third-harmonic generation from a single nanoslit [132]. © Turpion-Moscow Ltd. Used by permission.

cond laser. A 10^4 photon s^{-1} flux was obtained in the UV region from a single gold nanostructure in [132], where the third-harmonic generation in the UV region was studied with a nanostructure in the form of a nanoslit made in a gold/aluminum film. Such nanostructures are Babinet-complementary to nanorods, which are most often used in nanoplasmonics. As a nanorod, a nanoslit can have two plasmon resonances excited by radiation polarized along and perpendicular to the nanoslit [133].

Gold is the most popular plasmonic material. However, recent studies have shown that the optical nonlinearity of aluminum is much higher than that of gold. It was shown in [83, 126] that the susceptibility $\chi^{(3)}$ of aluminum at a wavelength of 1550 nm is three orders of magnitude higher than that of gold. At a wavelength of 780 nm, this difference is about two orders of magnitude [134]. Thus, nanostructures made of aluminum can be more efficient sources of third harmonics in the UV region than gold nanostructures. However, at a wavelength of 780 nm, although the susceptibility $\chi^{(3)}$ of aluminum is higher than that of gold, the observed field enhancement in the gold structure is greater than in the aluminum structure. This is explained by the fact that gold has better plasmonic properties at a wavelength of 780 nm than aluminum does [83, 126].

Figure 9 illustrates the UV emission spectra obtained from a nanoslit in a metal film. The third-harmonic spectrum is shown in Fig. 9b. The spectrum exhibits a peak at a wavelength of 260 nm, equal to 1/3 of the emission wavelength at the fundamental frequency. Measurements of the dependence of the third-harmonic power on the pump power showed that it is well approximated by a cubic dependence, which also confirms the observation of the third-harmonic generation. The frequency scale was calibrated by the UV emission spectrum of a mercury lamp transmitted through a single nanohole (Fig. 9a) [135].

The optical nonlinearity of an individual gold SHR nanostructure was studied in [18] for second- and third-harmonic generation in the UV spectral range. The high efficiency of generating harmonics in the UV range was achieved by using (i) ultrashort laser pulses (two cycles of the laser pulse wave) [136], (ii) ultrahigh laser intensity (near the air ionization threshold), (iii) nanostructures with the maximum nonlinear optical response, and (iv) SHR nanostructure surfaces with atomic-level homogeneity.

Generation at numerous frequencies was obtained from an SHR nanostructure. As shown in [102], plasmonic modes appear in the SHR structure for an established ratio of the hole diameter to the nanorod length, which determines the appearance of different multipole patterns in the nanostructure response. The number of excited modes is determined by the spectral width of the exciting laser radiation. The number of excited modes in small nanostructures is determined only by the nanostructure size, and this number is small. On the contrary, the number of excited modes in a large nanostructure can be considerable and, to excite them efficiently, the spectral width of laser radiation should be sufficiently large [18].

Figure 10 illustrates the nature of harmonic generation in an SHR nanostructure. A laser excites four plasmonic modes in the SHR nanostructure: the dipole mode ($\omega_1, \lambda_1 = 750$ nm), the $n = 3$ multipole mode (ω_2, $\lambda_2 = 770$ nm), the $n = 4$ multipole mode (ω_3, $\lambda_3 = 800$ nm), the $n = 5$ multipole mode (ω_4, $\lambda_4 = 880$ nm). The spectral dependences of the field intensity in these modes are presented in Fig. 10a. The high intensity and large spectral width of laser radiation (two cycles of the laser light wave) provide the simultaneous excitation of four multipole plasmonic modes in the SHR nanostructure.

The insets in Fig. 10a show numerical simulations (by the finite-difference time-domain (FDTD) method) of the near-field amplitude distributions for an SHR nanostructure illuminated by monochromatic radiation. These distributions confirm the multipole type of excited resonances.

The excitation of plasmonic modes results in an increase in the local field at the wavelengths λ_1, λ_2, λ_3, and λ_4 corresponding to these modes; the second and third

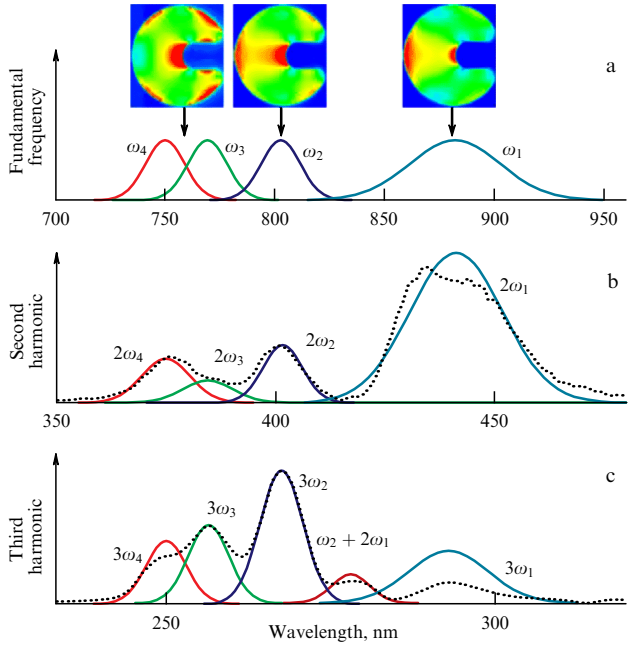

Figure 10. (Color online.) Second- and third-harmonic generation in the SNR nanostructure: (a) spectra of the ω_1, ω_2, ω_3, and ω_4 plasmonic modes and the corresponding calculated near-field distributions for the SHR structure, (b) experimental (dotted curve) and calculated second-harmonic generation spectra corresponding to excitation of the ω_1, ω_2, ω_3, and ω_4 plasmonic modes in the SHR nanostructure, (c) experimental and calculated third-harmonic generation spectra corresponding to excitation of the ω_1, ω_2, ω_3, and ω_4 plasmonic modes in the SHR nanostructure [18]. © American Chemical Society. Used by permission.

harmonics are therefore emitted at the doubled and tripled frequencies of these resonances. Figure 10b shows the second-harmonic spectrum and the calculated second-harmonic spectra corresponding to the excitation of plasmonic modes ω_1, ω_2, ω_3, and ω_4 in the SHR structure. Figure 10c presents the third-harmonic spectrum and the calculated third-harmonic spectra corresponding to excitation of plasmonic modes ω_1, ω_2, ω_3, and ω_4. The peak power was $I_{3\omega,\,\mathrm{peak}} = 3.4 \times 10^7$ W cm^{-2}, while the radiation field amplitude at the third-harmonic frequency was a considerable part of the field amplitude at the fundamental frequency: $E_{3\omega} = 0.006E_{\omega}$. At present, such a nanolocalized UV radiation source is providing record high intensity and light-conversion efficiency with the UV photon flux 4×10^8 photon s^{-1} [18].

4. Photoluminescence of a single nanostructure

4.1 One-photon photoluminescence

Photoluminescence (PL) of noble metals is underlain by two physical mechanisms. The first is an interband transition involving excitation of an electron from the valence band to the conduction band [95]. In this case, PL in a metal can be described as a three-stage process: (i) excitation of electrons and generation of electron–hole pairs, (ii) scattering of electrons and holes with a partial energy transfer to lattice phonons, and (iii) electron–hole recombination with the emission of a photon. The second mechanism is an intraband transition in which the excitation of electrons is described in the model of absorption of radiation by almost free electrons. In this process, one photon is absorbed by an electron in the presence of a third particle (for the energy and momentum conservation laws to be satisfied) [137]. Photoluminescence was first discovered from a gold surface in 1969 [95].

Photoluminescence from noble metals covers a broad spectral range from the IR to the UV [137]. The physics of the formation of such an extremely broad luminescence spectrum lies in the nature of the electron–phonon mechanism of radiation absorption by metals. The PL phenomenon has been extensively studied in different metals [138]. At present, interest in the PL of gold is related, in particular, to the possibility of using gold nanoparticles as theragnostic biomarkers. Photoluminescence allows simultaneously performing microscopy and local heating of a tissue for photodynamic therapy [139]. Until the advent of technologies for manufacturing nanostructures, the possibility of practical applications of PL remained uncertain because of the extremely low PL efficiency: the quantum yield of PL from a metal surface is of the order of 10^{-10} [95].

The absorption of radiation in a metal followed by PL can occur only within a skin layer, i.e., at the nanoscale. Therefore, with the development of technologies for manufacturing nanostructured objects, interest in PL was revived, but now for nanostructures. The extremal increase in the quantum yield of PL from nanoobjects has been demonstrated. For example, a quantum yield of PL of the order of 10^{-6} was obtained for spherical nanoparticles [140]. The quantum yield of PL from nanorods reaches 10^{-4} [141]. The dramatic increase in the PL intensity in gold nanoobjects was explained by a mechanism involving the absorption of a photon and excitation of an electron at the interband d–sp transition, followed by a nonradiative recombination of the excited holes in the d band with the sp electrons, with the excitation of a plasmon in the nanoparticle. These localized plasmons are a source of efficient PL [96].

Spherical nanoparticles demonstrate size-independent PL. This is explained by the fact that the photon emission rate, proportional to R^{-3}, is exactly compensated by the same dependence $\sim R^{-3}$ of the radiative decay rate. Photoluminescence also depends on the nanoparticle polarizability [142], which in turn depends on the nanoparticle size and geometry. The PL efficiency for Au nanorods is higher than that for spherical Au nanoparticles because of excitation of plasmon resonances with a considerably higher polarizability [140].

Photoluminescence from a nanohole in a metal screen is of interest for the creation of a nanolocalized radiation source. As shown in [97], PL from a single nanohole allows realizing a nanolocalized radiation source with the following properties: (i) an extremely wide emission spectrum, (ii) a high quantum yield of PL, (iii) the source can be narrowband and tunable in a broad spectral range.

The PL mechanism in gold nanostructures and nanoholes in a gold film is the same (Fig. 11) and differs from the PL mechanism in a gold film. This is manifested in the difference of PL spectra from nanoholes and from the metal film surface [97]. Photoluminescence in a gold film appears upon excitation and the subsequent recombination of an electron–hole pair accompanied by the emission of a PL photon [96]. Photoluminescence of nanoobjects appears upon excitation of localized plasmons. Figure 11b shows that the maximum PL signal for nanoholes corresponds to a plasmon resonance

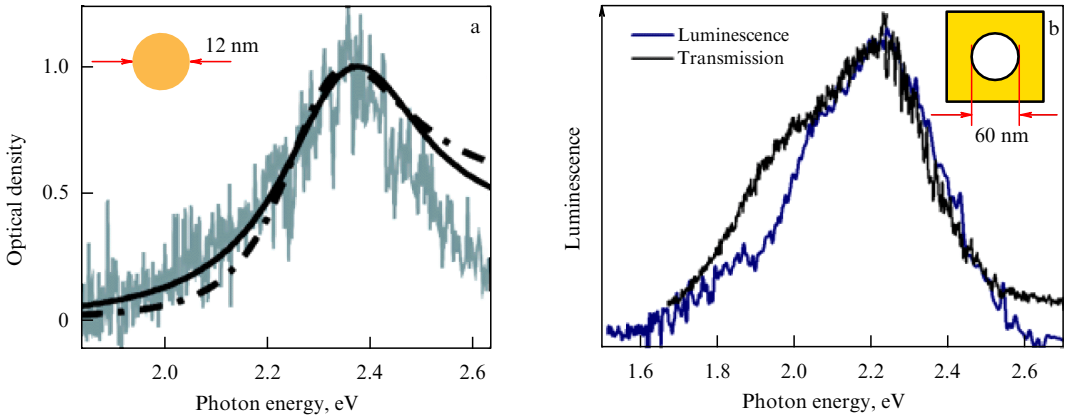

Figure 11. Comparison of PL from gold nanostructures: (a) optical density (black curve) and PL (grey curve) measured for gold nanospheres 12 nm in diameter; the dashed-dotted curve shows the corresponding extinction spectrum calculated using the Mie theory [96]; (b) experimental transmission and PL spectra of a nanohole 60 nm in diameter in a 200 nm gold film [97]. In both cases, the PL maximum is close to the plasmon resonance. © American Physical Society and OSA. Used by permission.

($\approx$ 2.2 eV, 550 nm) in a nanohole made in a gold film. The spectral properties of this resonance are presented in Fig. 11b. The peak energy of PL photons for a gold film is related to the energy difference between excited holes in the d band and electrons on the Fermi surface, which is approximately 1.8 eV (690 nm) near the X symmetry point of the first Brillouin zone in gold and 2.4 eV (510 nm) near the L symmetry point [137].

The PL efficiency from a nanohole is considerably higher than from a gold film. Measurements showed that the PL quantum yield for holes from 20 nm to 1 μm in diameter is about 10^{-6}, which is approximately 10^4 times higher than for PL from a gold film surface [97]. These data are in good agreement with PL measurements for spherical gold nanoparticles [96].

4.2 Multiphoton-induced photoluminescence

The resonance behavior of oscillations of free electrons in an exciting optical field in metal nanostructures makes the nonlinear multiphoton PL possible. The probability of this process on a smooth gold surface is extremely low, and nonlinear multiphoton-induced PL has not been observed on a smooth surface so far.

Among nonlinear PL processes, the two-photon process (2PPL) in gold nanoparticles is studied most thoroughly. Figure 12a shows the excitation scheme in a gold nanoparticle by radiation at 780 nm [143]. The first photon excites an electron at the intraband transition in the sp conduction band (*1*). The second photon excites an electron from the d band, which recombines with the sp hole in the conduction band (*2*). Photoluminescence appears due to the two-photon process involving the production of a hole in the d band followed by its recombination with an electron from the sp band. Because of the increased density of states, the interband radiative recombination in 2PPL occurs, as in usual PL, near the L and X points of the reciprocal space, resulting in two emission bands in the respective green and red spectral regions [143]. The 2PPL dynamics are determined by the relaxation time of the distribution of carriers excited in the sp conduction band after the absorption of the first photon. This time lies in the picosecond range [143].

As mentioned above, the nonlinear PL efficiency can be considerably increased using a plasma resonance of a nanostructure. In addition, the radiative transition rate can be changed by changing the optical properties of the environment. Thus, the increase in the PL emission rate in a

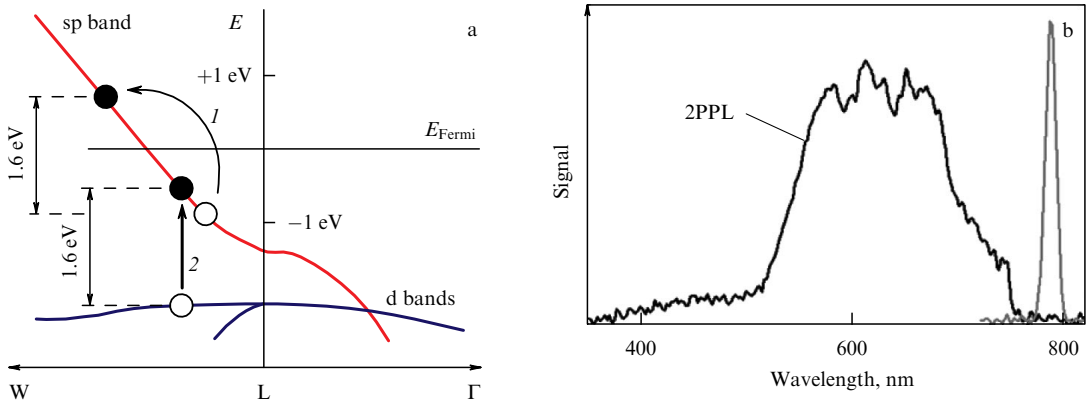

Figure 12. Two-photon luminescence in gold. (a) band structure of gold near the L symmetry point of the first Brillouin zone. Multiphoton excitation transfers an electron from the d to sp band. After the nonradiative relaxation of a hole and an electron, electron–hole recombination can occur with spontaneous photon emission (photoluminescence). (b) Experimental two-photon PL spectrum (black curve); the grey curve shows the exciting laser line [101]. © OSA. Used by permission.

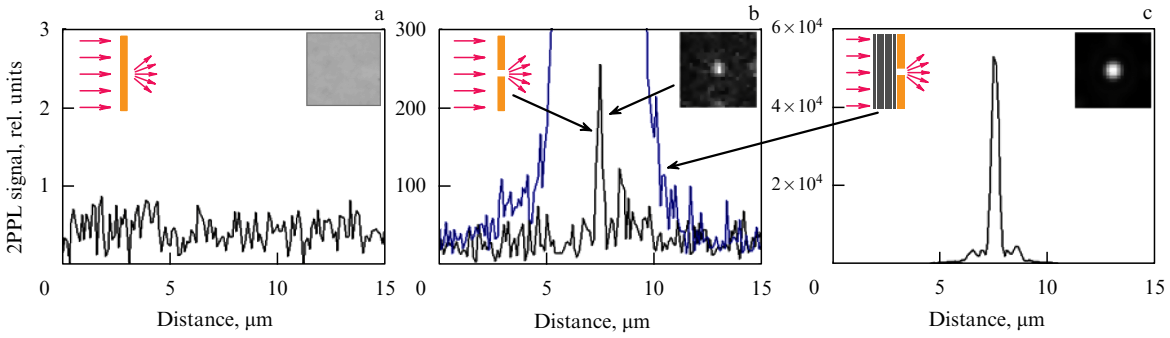

Figure 13. (Color online.) 2PPL of a nanofilm and a single nanohole for the same parameters of exciting laser radiation: (a) 2PPL from a nanofilm; (b) 2PPL from a nanohole in a metal nanofilm (black curve) and 2PPL from a nanohole in a PC–metal nanofilm system (blue curve); (c) 2PPL from a nanohole in the PC–metal nanofilm system at full scale. Insets show excitation schemes and corresponding two-dimensional images [101]. © OSA. Used by permission.

metal nanoobject was demonstrated in [101] when three physical effects were *simultaneously* involved in this process: (i) the size effect, (ii) plasmon resonance, and (iii) an optical Tamm state (OTS). A single nanohole in a metal film deposited on a photonic crystal was studied as a luminescent nanoobject.

The surface of a photonic crystal (PC) was covered with a gold nanofilm in which a nanohole was produced. Upon illumination of the PC–nanofilm system by resonance optical radiation, an OTS is excited on the inner surface of the metal film [144]. The nanohole is immersed in the electromagnetic OTS mode. Such a scheme can provide not only the surface localization of the electromagnetic field but also its considerable enhancement compared to the light field strength incident on the PC–metal nanofilm system [62].

It is well known that the plasmonic mechanism of field enhancement is based on the fast response of the electron subsystem of a metal with the characteristic time of a few femtoseconds [145]. The physical nature of the OTS appearance mechanism is different and is based on the constructive interference of electromagnetic waves in a PC. The OTS formation time is determined by the Q factor of the corresponding OTS resonance and lies in the range between 150 and 200 fs [145]. To simultaneously realize (i) the plasmonic mechanism of electromagnetic field enhancement and (ii) the OTS electromagnetic field enhancement, the exciting pulse duration should be about a picosecond. In experiments in [101], 1.2 ps laser pulses tunable in the 700–900 nm spectral range were used.

Figure 12b presents the multiphoton luminescence spectrum measured from a single nanohole 60 nm in diameter made in an Au film on a quartz substrate irradiated by 10 mW laser pulses. The right narrow peak corresponds to the exciting radiation. The peak of the PL spectrum is located at a wavelength of 570 nm and approximately corresponds to the forbidden band energy of gold near the L symmetry point of the first Brillouin zone (550 nm). The short-wavelength wing extends to 380 nm. The multiphoton PL intensity is quite well approximated by a quadratic dependence.

Figure 13 illustrates the increase in the multiphoton PL intensity. The insets in Fig. 13 show laser-excitation schemes of nanoholes and corresponding two-dimensional images. Figure 13a shows the results of 2PPL measurements from an extremely smooth gold nanofilm. The 2PPL signal was not detected in experiments because of its weakness. The 2PPL from a smooth gold film is absent because intraband dipole transitions are forbidden in the metal. The quantum yield of 2PPL from a smooth gold surface is estimated as no more than 10^{-13} for a 1 mW radiation power.

Figure 13b shows the results of similar measurements for a gold film with a nanohole, and Fig. 13c shows results for a nanohole in a PC–metal nanofilm system. The size effect (nanohole) leads to considerable enhancement of PL (Fig. 13b). The measured quantum yield of 2PPL was 10^{-9}. The placement of the nanohole into the OTS mode results in a further significant amplification of the PL signal, by more than 200 times compared to the nanohole. Figure 13b shows the PL signal from the nanohole in the gold film (black curve) and the PL signal from the nanohole in the PC–metal nanofilm system (blue curve).

Thus, in the example of the 2PPL of a gold nanoobject placed near a PC supporting the OTS at the PL excitation wavelength, the enhancement of the radiative capability of a nanoobject by a factor of 10^6 upon simultaneous realization of three effects was demonstrated. One of the possible practical applications of 2PPL is the creation of nanolocalized broadband radiation sources [146].

5. Applications

5.1 Optical diode

Among optical systems for nanoscale light control [147, 148], so-called optical diodes are important, in which the light transmission coefficient depends on the light propagation direction. In optical diodes, different physical effects are used to obtain asymmetric light propagation. Most often, the asymmetry is obtained by using elements in which the permittivity (1) is a nonsymmetric tensor (due to the Faraday effect) [147], (2) depends nonlinearly on the exciting field strength [149], and (3) explicitly depends on time [150, 151]. Such devices are nonreciprocal because the Lorentz reciprocity theorem is violated [152].

There is a class of optical systems satisfying the Lorentz reciprocity theorem but having different transmissions for light incident on them from different sides (so-called light propagation asymmetry). As was shown in [153], such devices cannot be considered optically nonreciprocal. However, some of them can be used for constructing optical diodes [154].

The light propagation asymmetry can be obtained by using planar structures and linearly polarized light. Planar structures can efficiently convert one linear polarization into

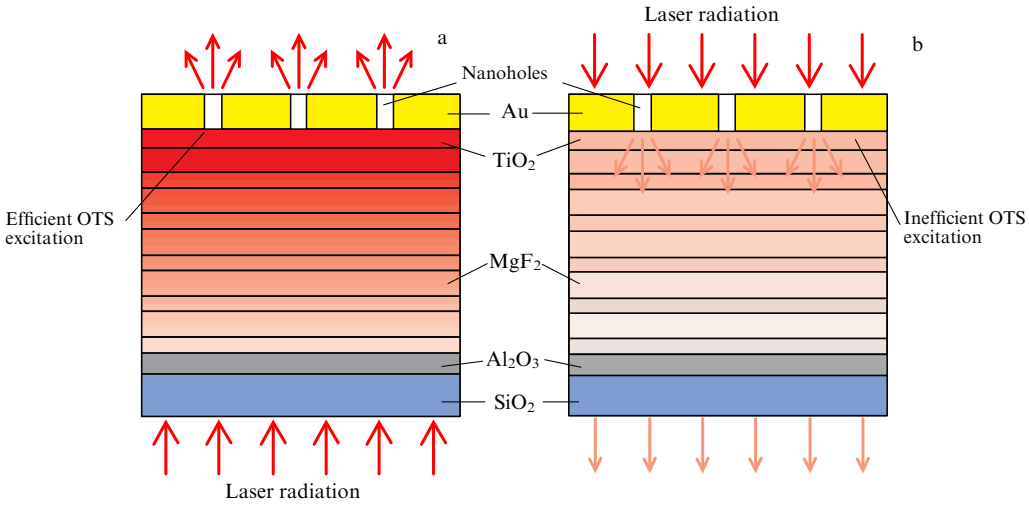

Figure 14. (Color online.) Schematic geometry and operation principle of an optical diode consisting of a metal array of nanoholes on the surface of a planar PC. (a) Light is incident on the PC side, (b) light is incident on the metal film side [157]. © American Physical Society. Used by permission.

another [155, 156]. The propagation of light with the chosen polarization in such systems depends on the irradiation direction, which means the asymmetry of polarized light propagation.

Another example of using a planar structure to achieve light propagation symmetry is a planar optical system [157] consisting of an array of nanoholes in a metal film deposited on the surface of a planar PC, as shown schematically in Fig. 14.

The optical structure is an array of holes in a metal nanofilm deposited on the surface of a planar dielectric nonmagnetic PC (metasurface). The PC consists of dielectric layers and has a forbidden band for the transmission of light propagating normally to its layers. The deposition of a metal film on the PC surface results in the formation of a specific feature in the transmission spectrum: a narrow transmission peak appears in the forbidden band of the PC. The transmission peak appears due to a break in the translation symmetry of the PC caused by the metal film. The optical electromagnetic field mode at the interface of metal–dielectric periodic structures is called the OTS in the literature [62–64, 158, 159].

In the optical-diode geometry under study, noticeable transmission is achieved only at wavelengths corresponding to the OTS excitation. In this case, the mechanism of light propagation asymmetry is as follows. When light is incident on the optical diode from the PC side, the OTS is excited (the case of direct propagation in the diode-related terminology), and this in turn leads to the efficient transmission of light through nanoholes in the metal nanofilm. When a plane wave is incident from the gold film side (the case of backward propagation in the diode-related terminology), an OTS can be excited by light propagated through nanoholes. Nanoholes significantly change the wavefront of the incident plane wave and the light incident on the PC is unmatched with the OTS mode, and the latter is therefore excited inefficiently. This leads to the inefficient transmission of light through nanoholes. It is the *difference in the OTS excitation efficiencies* that leads to a strong asymmetry in light transmission.

Figure 15 demonstrates the optical asymmetry of a metasurface. Figure 15 shows optical-microscope images of

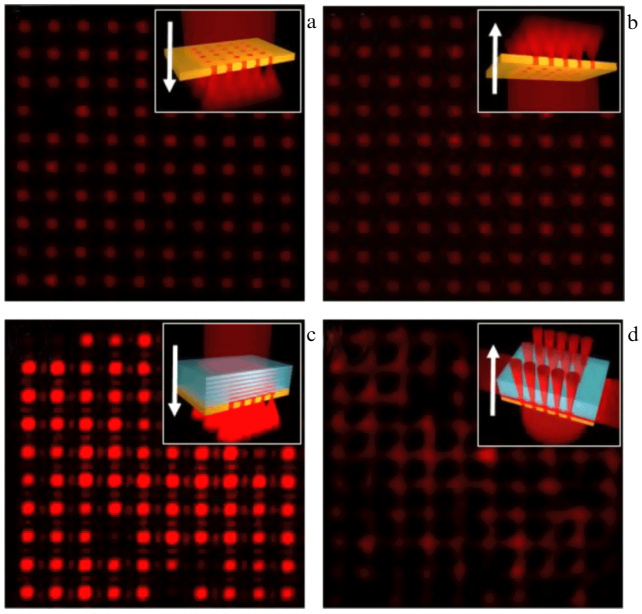

Figure 15. (Color online.) Asymmetry in the light transmission by a metasurface. The images of a control gold perforated nanofilm (a, b) and metasurface (c, d) illuminated by laser light. Insets show the incident light direction. For a simple gold film (a, b), the change in the radiation direction does not change the transmission of light. For the metasurface, the transmission of light highly depends on the radiation direction. © American Physical Society. Used by permission.

a gold perforated nanofilm (Fig. 15a, b) and a metasurface (Fig. 15c, d) obtained with the help of a CCD array camera. The gold nanofilm and the metasurface were illuminated by a 795 nm laser beam. Insets in the figures show the incident light direction with respect to the surface of the samples. We can see that in the case of a simple gold film sample (Fig. 15a, b), a change in the light direction does not change the light transmission. For the metasurface, the light transmission greatly depends on the light direction: when light is incident from the PC side (Fig. 15c), each nanohole is a bright light source. When light is incident from the gold nanofilm side, only weak radiation from each nanohole is

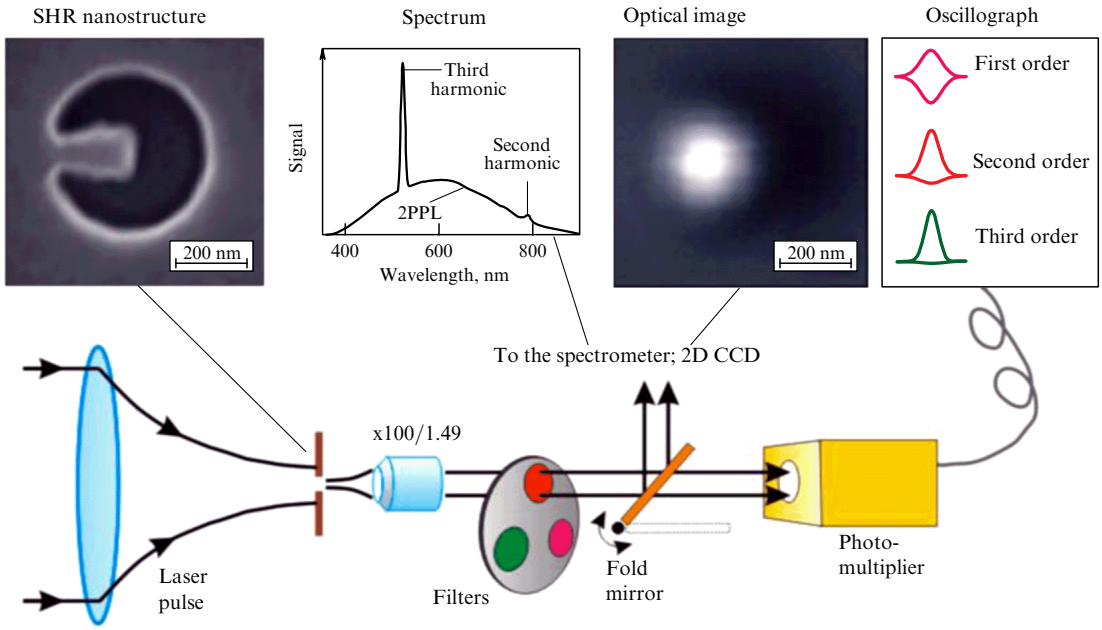

Figure 16. (Color online.) Principal scheme for measuring the spatiotemporal properties of femtosecond laser radiation with the help of a single plasmonic SHR nanostructure. Top, left to right: electron microscope image of the SHR nanostructure, emission spectrum of the SHR nanostructure excited by a 1560 nm laser line, and an optical image of the SHR nanostructure at the third-harmonic wavelength [167]. © IOP Publishing. Used by permission.

observed. Figure 15c, d conclusively demonstrate the metasurface nonreciprocity effect.

5.2 Nanoprobe of a femtosecond laser pulse

At present, measuring ultrashort femtosecond optical fields with a nanometer spatial resolution is still a difficult problem. Such measurements are fundamentally important both for understanding the spatiotemporal dynamics of ultrashort pulses [160] and for many scientific and practical applications, such as the study of the interaction of light with matter on the nanoscale [161, 162].

It is well known that all the parameters of a laser pulse $E(t)$ can be determined by measuring autocorrelation functions $G_n(\tau)$ of all orders [160]. Higher-order correlation functions can be obtained experimentally using multiphoton processes. In practice, only the second-order correlation function is typically measured and then the results are analyzed assuming *a priori* knowledge of the laser pulse shape. The method of measuring the second-order autocorrelation function gives limited information on the pulse duration and shape and only higher-order correlations are sensitive to the pulse asymmetry [163]. However, most methods based on higher-order correlations have a low sensitivity and a limited time resolution, and are complicated in practice. Modern methods for measuring laser pulse parameters include the autocorrelation method, frequency-resolved optical gating (FROG), and spectral phase interferometry for the direct reconstruction of the pulse electric field shape [160].

Measuring an ultrashort optical pulse with a *nanoscale* spatial resolution is an even more complex problem. The interferometric method with an optical fiber used for studying ultrashort laser pulses was presented in [164]. Laser pulses were analyzed using nonlinear nanocrystals on substrates [165] and a nonlinear nanoprobe consisting of a tapered silica fiber, a nanowire, and nonlinear fluorescent spheres [166].

It is well known that the localization of an electromagnetic field in a metal nanostructure is determined by its size and can be of the order of a few nanometers. This value determines the effective size of a metal nanoprobe. The time scale of the surface plasmon dynamics is a few hundred attoseconds [6], determining the subfemtosecond time resolution of the nanoprobe. High-intensity laser radiation efficiently interacts nonlinearly with a nanostructure generating harmonics. The emission of harmonics can be used for autocorrelation measurements of the duration of the laser pulse exciting the nanostructure. Optical near fields corresponding to the second- and third-harmonic generation are localized on the nanometer scale and therefore the effective size of the probe is also a few nanometers.

The spatiotemporal properties of femtosecond laser pulses were studied in [167] using a nanoprobe based on an SHR nanostructure. The nanostructure was made on a 100 nm thick aluminum film deposited on an ultrathin 40 nm thick membrane with the help of a tightly focused ion beam [102]. The dimensions of the nanostructure were chosen so as to obtain the maximum enhancement of the near-field amplitude at the fundamental frequency [102]. The emission of the SHR structure excited by a 1560 nm laser line contains the second and third harmonics (Fig. 16). An optical image of the SHR structure at the third-harmonic wavelength is also shown in Fig. 16.

Autocorrelation measurements were performed with a Michelson interferometer. The setup for measuring the spatiotemporal properties of femtosecond laser radiation with the help of a single plasmonic SHR structure is shown in Fig. 16. After the interferometer, two pulses were directed to a microscope and focused on the SHR structure. The fundamental-frequency radiation transmitted through the nanostructure and the third- and second-harmonic radiation were collected on a detector. The fundamental radiation transmitted through the nanostructure was used for first-order autocorrelation measurements, the second-harmonic

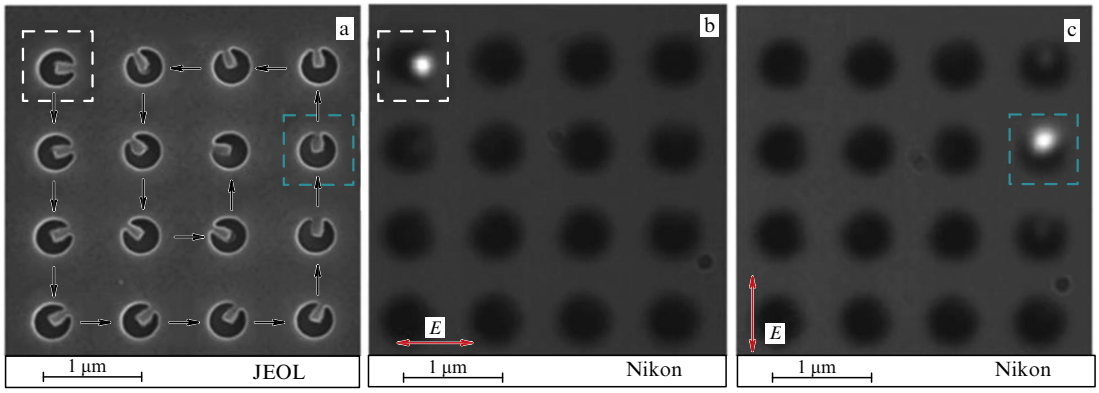

Figure 17. (Color online.) All-optical SHR nanostructure display. (a) Electron microscope image of the optical display: SHR nanostructures are made in a 50 nm thick aluminum film in the form of a 4 × 4 array with a step of 1 μm. (b) Optical microscope image of the optical display illuminated by radiation polarized along the nanorod of the first SHR nanostructure (shown by the yellow frame). (c) Optical microscope image of the optical display illuminated by radiation polarized along the nanorod of the SHR nanostructure (shown by the blue frame). The red arrows show the direction of polarization of the exciting radiation [128]. © IOP Publishing. Used by permission.

radiation for second-order autocorrelation measurements, and the third-harmonic radiation for third-order autocorrelation measurements. Thus, the SHR nanoprobe allows measuring the duration of femtosecond pulses with nanometer spatial resolution.

5.3 All-optical nanodisplay

The anisotropy of nanostructure geometry implies the dependence of its optical response on the polarization of incident radiation. The SHR nanostructure geometry has a distinct anisotropy determined by the direction of its nanorod, which implies the polarization-dependent optical response of the SHR nanostructure to the external laser field [128].

Theoretical calculations of the near-field distribution for an SHR nanostructure excited by a laser showed that a change in the radiation polarization from parallel to the one orthogonal to the nanorod leads to a change in the fundamental radiation intensity by a factor of 50. However, for the same change in polarization, the third-harmonic power increases by 40,000 times (see Fig. 8) [128]. Such a strong dependence of third-harmonic generation of the SHR nanostructure on the laser polarization can find important practical applications in optical sensors and ultrafast optical switches. The use of SHR nanostructures for creating a prototype of the *all-optical display* with SHR nanostructures as 'pixels' was demonstrated in [128]. The optical display is an array of SHR nanostructures separated by 1 μm (Fig. 17). The size of the optical display is determined by the minimal distance between nanostructures, which was 500 nm (1/3 of the excitation wavelength). The nanostructures are made in a 50 nm thick aluminum film. The direction of the nanorod in each SHR nanostructure is turned with respect to the neighboring nanostructure through 11.5° (Fig. 17a). Such an optical display operates as follows. All the SHR nanostructures are illuminated by 1.56 μm femtosecond pulses. When radiation is polarized along the nanorod of one of the SHR nanostructures, this nanostructure is in exact resonance with the laser field and becomes an efficient third-harmonic source. Thus, choosing a certain direction of the radiation polarization vector allows 'switching on' certain 'pixels' of the display.

Figures 17b, c illustrate the operation of an optical nanodisplay. The nanodisplay is illuminated by a femtosecond laser pulse. Under rotation of the polarization vector, a resonance with one of the SHR structures of the display appears, and this SHR structure becomes a third-harmonic radiation source. For example, to address the first pixel of the display (the yellow dashed square in Fig. 17a), the polarization vector is chosen along the nanorod of this SHR structure. The display illumination then leads to the emission of only this pixel (Fig. 17b). When the polarization vector is turned so as to coincide with the direction of the nanorod in another SHR structure (the blue dashed square in Fig. 17a), it becomes resonant with the incident radiation and the emission of only that pixel appears (Fig. 17c).

5.4 Thermoplasmonics

The field of nanoplasmonics studying the heat release in nanoparticles caused by laser irradiation is called *thermoplasmonics*. Thermoplasmonics has found practical applications in medicine and biology.

5.4.1 Cancer cell therapy [168]. This new type of therapy is based on achieving an optical contrast in absorption between cancer and healthy tissues. A metal nanoparticle can be selectively attached to an ill cell and irradiated by laser light. Heating the nanoparticle by light allows its use for therapy by damaging ill cells without touching healthy tissue [82, 169]. Among the available photothermal agents, plasmon nanoparticles are the best candidates for selective photodamage using moderate laser radiation intensities. The greatest positive effect is achieved with gold nanorods and nanoshells because they can be efficiently heated by radiation at wavelengths in the so-called 'biological transparency window' in the near-IR region [170].

5.4.2 Nanosurgery. A laser beam can be used as a tool for the transfection of individual cells by forming a transient pore in a cell membrane with the help of a heated nanoparticle, which allows introducing either therapeutic agents (proteins, LNA, RNA) or visualization agents (fluorophores, quantum dots, nanoparticles) into the cell through the cell membrane [171, 172].

5.4.3 Targeted transport of drugs. Another biomedical application in thermoplasmonics involves the targeted trans-

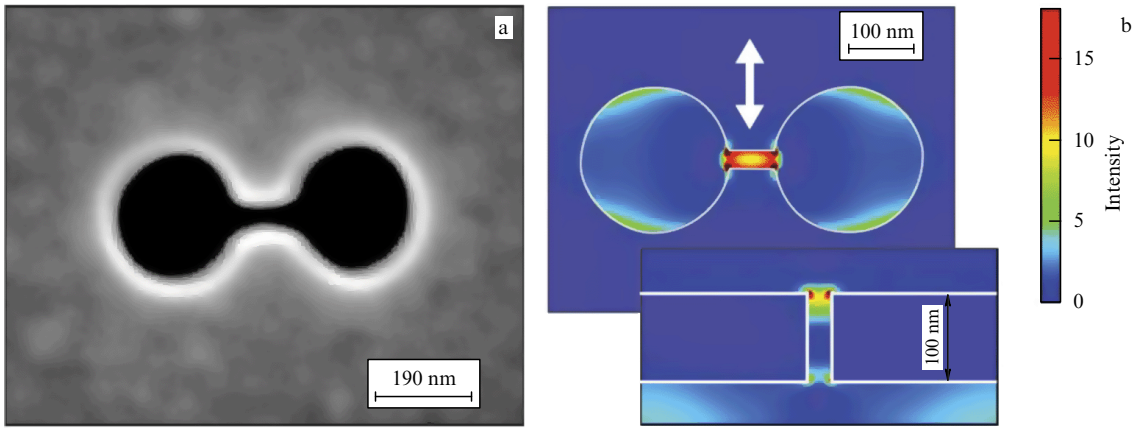

Figure 18. (Color online.) Plasmonic DNH structure: (a) electron microscope image of a structure produced in a 100 nm gold nanofilm by a tightly focused ion beam, (b) near-field amplification (linear scale) for a DNH nanostructure formed by nanoholes 633 nm in diameter and a 25 nm gap illuminated by a 633 nm laser line linearly polarized perpendicular to the slit connecting nanoholes. The inset shows the intensity amplification along the vertical cut at the center of the DNH structure [180]. © Nature Publishing Group. Used by permission.

port of drugs or genes for therapy. Therapeutic agents are attached to gold nanoparticles serving as nanocarriers in a human body. After the transport of the therapeutic agent to the required site, they can be detached and released using the remote laser heating of a nanoparticle [173].

5.4.4 Photothermal visualization. Thermoplasmonics is used in photothermal visualization. Upon irradiation of a metal nanoparticle, the temperature of the environment increases, resulting in a local change in the refractive index. The local change in the refractive index (the nanolens effect) can be detected by interferometric measurements [70, 174].

Visualization is also possible using acoustic waves [175]. Photoacoustic tomography is based on the generation of acoustic signals by short laser pulses. The absorption of laser pulses by a nanoparticle causes a localized rapid increase in temperature. The subsequent thermal expansion of the tissue causes the formation and propagation of acoustic waves, which can be detected with acoustic sensors.

5.4.5 Nanolevel control of chemical reactions. Thermoplasmonics has become an efficient method for the nanolevel control of chemical reactions. According to the empirical Arrhenius law, the chemical reaction rate constant K depends on the temperature T as

$$K = A \exp\left(-\frac{E_a}{k_B T}\right), \tag{45}$$

where A is a constant, E_a is the activation energy, and k_B is the Boltzmann constant. The possibility of controlling the heat release with an unprecedented spatial and temporal accuracy is regarded as an efficient tool for the nanolevel control of chemical reactions [176].

5.5 Nonlinear microscopy

An important application of the generation of harmonics from nanoobjects is nonlinear microscopy. One of the motivations for using nonlinear effects, in particular, harmonic generation, is to improve the transverse and longitudinal resolution of optical microscopy. The resolution increases because nonlinear processes proceed most efficiently in the region of maximum intensity of a focused laser beam. Another advantage of microscopy based on harmonic generation is that the wavelength of the harmonics is far from the wavelength of the background signal that arises from the scattering of laser light [177].

5.6 Optical tweezers based on a single plasmonic nanostructure

The ability to concentrate light in a very small volume opens up fundamentally new ways to manipulate nanoobjects with the help of so-called optical tweezers. In conventional optical tweezers, micro- and nanoparticles are localized by a gradient force appearing in the focal region of the laser beam [178]. The accuracy of controlling the spatial position of micro- and nanoparticles by optical tweezers is determined by the waist size of the laser beam at the focus of the microscope objective and, in the best case, is a fraction of the laser wavelength [179].

Plasmonic structures can be used to localize the light field in the nanometer range [8, 16, 47] and apply it to create optical tweezers [181]. In [182], optical tweezers were proposed based on a single plasmonic structure in the form of two nanoholes connected with a nanoslit, which was called a 'double nanohole' (DNH) (Fig. 18). The nanostructure was made in a thin metal nanofilm. A specific feature of this nanostructure is the combination of strong field enhancement and the efficient suppression of laser radiation that excites plasmonic resonances in nanostructures in the form of nanoholes. The DNH structure exhibits resonance properties determined by its geometry, its diameter, and the distance between nanoholes [183]. As shown in [180], such a structure can localize light within a volume of 70 zl (10^{-21} l), which is approximately 7000 times smaller than the diffraction-limited volume obtained in an optical microscope.

The possibility of trapping dielectric nanoparticles with the help of DNH optical tweezers was demonstrated in [184]. Figure 19a presents an optical tweezer scheme. The nanostructure was made at the end of an optical fiber [185]. First, a gold film was deposited on the fiber end, in which a DNH nanostructure was created with the help of a tightly focused ion beam. The fiber end with the DNH structure was then immersed in an aqueous solution of dielectric nanoparticles (polystyrene nanospheres 20 nm in diameter). Into the other end of the fiber, laser radiation at 980 nm was coupled, which produced a spatially localized field near the DNH nano-

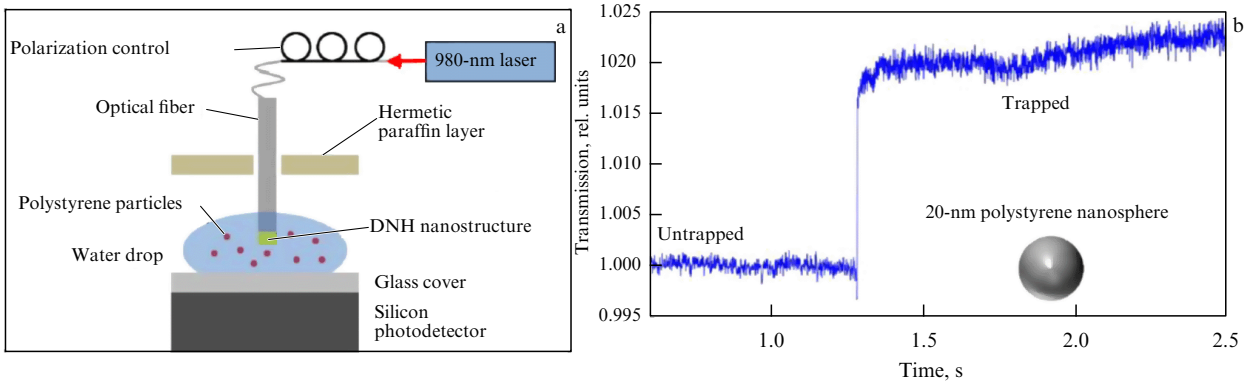

Figure 19. (Color online.) Localization of nanoparticles with the help of a DNH nanostructure. (a) Schematic of the experimental setup using a DNH nanostructure produced at the fiber end. Upon localization of the nanostructure, the light transmission through the DNH increases. (b) Example of the localization of polystyrene nanospheres 20 nm in diameter at the optical nanofiber end where the DNH nanostructure was made. A large increase in transmission through the DNH structure by 2% demonstrates the trapping of a nanoparticle near the DNH nanostructure [184]. © IOP Publishing. Used by permission.

structure, capable of trapping dielectric nanoparticles. The localization of a nanoparticle was controlled by a change in the transmission of light through the DNH nanostructure: as a nanosphere is trapped, the transmission of light through the DNH increases. Figure 19b shows an example of localizations of polystyrene spheres. The increase in the transmission of light through the DNH structure by 2% demonstrates the trapping of a nanosphere. The confinement time of such a nanosphere in optical tweezers was a few minutes. Optical tweezers were used to localize nanosphres 20 nm in diameter made of different materials to measure their Raman spectra [186], to localize magnetic nanoparticles [187], and to trap and study single DNA molecules [188].

6. Conclusions

The advances in experimental techniques allow studying single nanostructures. Measurements at the level of *single* nanostructures can be efficiently used to study the fundamental optical and spectroscopic properties of nanostructures determining the elementary physical mechanisms responsible for processes occurring in them. They also exclude averaging inherent in experiments with ensembles of particles, in which physical information on the parameters of nanoparticles such as the absorption cross section, the quantum yield of emission, and the polarization radiation and absorption anisotropy are inevitably lost.

A single plasmonic nanostructure has a number of unique properties, such as a small size, the possibility of light field amplification due to excitation of plasmonic resonances, and high optical nonlinearity. The optical and spatial properties of plasmonic resonances are directly related to material and geometric parameters of the nanostructures and the environment. The study of the properties of single plasmonic nanostructures is of interest not only from the general physical standpoint but also for practical applications in biology, catalysis, quantum optics, and information technologies.

We conclude that the development of optical methods for detecting and analyzing single nanostructures plays a key role in fundamental and applied nanotechnology studies. The use of single plasmonic structures allows studying the optical properties of metals at the nanoscale, the structure of their electron levels, including quantum effects, and various types of optical nonlinear interactions.

Acknowledgments

The work was supported by the Russian Science Foundation (contract no. 14-12-00729).

References

1. Kauranen M, Zayats A V *Nature Photon.* **6** 737 (2012)
2. Lapine M, Shadrivov I V, Kivshar Yu S *Rev. Mod. Phys.* **86** 1093 (2014)
3. Balykin V I *Phys. Usp.* **57** 607 (2014); *Usp. Fiz. Nauk* **184** 656 (2014)
4. Moerner W E *Rev. Mod. Phys.* **87** 1183 (2015)
5. Brongersma M L, Shalaev V M *Science* **328** 440 (2010)
6. Stockman M I et al. *Nature Photon.* **1** 539 (2007)
7. Jackson J D *Classical Electrodynamics* 3rd ed. (New York: Wiley, 1999)
8. Maier S A *Plasmonics*: *Fundamentals and Applications* (Berlin: Springer, 2007)
9. Kloos T *Z. Phys. A* **265** 225 (1973)
10. Höhberger H J, Otto A, Petri E *Solid State Commun.* **16** 175 (1975)
11. Petri E, Otto A *Phys. Rev. Lett.* **34** 1283 (1975)
12. Ritchie R H *Phys. Rev.* **106** 874 (1957)
13. Stern E A, Ferrell R A *Phys. Rev.* **120** 130 (1960)
14. Tanner D B "Optical effects in solids" (Gainesville, FL: Department of Physics, Univ. of Florida); https://www.phys.ufl.edu/˜tanner/notes.pdf
15. Osborn J A *Phys. Rev.* **67** 351 (1945)
16. Bohren C F, Huffman D R *Absorption and Scattering of Light by Small Particles* (New York: Wiley, 1998)
17. Khlebtsov B N, Khlebtsov N G *J. Phys. Chem. C* **111** 11516 (2007)
18. Melentiev P N et al. *Nano Lett.* **16** 1138 (2016)
19. Kreibig U, Vollmer M *Optical Properties of Metal Clusters* (Berlin: Springer, 1995)
20. Fuchs R, Claro F *Phys. Rev. B* **35** 3722 (1987)
21. Lal S, Link S, Halas N J *Nature Photon.* **1** 641 (2007)
22. González A L, Reyes-Esqueda J A, Noguez C *J. Phys. Chem. C* **112** 7356 (2008)
23. Flytzanis C et al., in *Progress in Optics* Vol. 29 (Ed. E Wolf) (Amsterdam: North-Holland, 1991) p. 321
24. Baida H et al. *Nano Lett.* **9** 3463 (2009)
25. Voisin C et al. *J. Phys. Chem. B* **105** 2264 (2001)
26. Otto A *J. Raman Spectrosc.* **22** 743 (1991)
27. Hu M et al. *J. Mater. Chem.* **18** 1949 (2008)
28. Blaber M G *J. Phys. Chem. C* **116** 393 (2012)
29. Juvé V et al. *Nano Lett.* **13** 2234 (2013)
30. Naik G V, Shalaev V M, Boltasseva A *Adv. Mat.* **25** 3264 (2013)
31. Link S, El-Sayed M A *J. Phys. Chem. B* **103** 8410 (1999)

32. Lindfors K et al. *Phys. Rev. Lett.* **93** 037401 (2004)
33. Berciaud S et al. *Nano Lett.* **5** 515 (2005)
34. Scholl J A, Koh A L, Dionne J A *Nature* **483** 421 (2012)
35. Sperling R A et al. *Chem. Soc. Rev.* **37** 1896 (2008)
36. Anker J N et al. *Nature Mater.* **7** 442 (2008)
37. Akimov A V et al. *Nature* **450** 402 (2007)
38. Born M, Wolf E *Principles of Optics* (Cambridge: Cambridge Univ. Press, 2002)
39. Jain P K et al. *Plasmonics* **2** 107 (2007)
40. Garcia M A *J. Phys. D* **44** 283001 (2011)
41. Sarychev A K, Shalaev V M *Electrodynamics of Metamaterials* (Singapore: World Scientific, 2007)
42. Kumar C S S R (Ed.) *Nanostructured Thin Films and Surfaces* (Nanomaterials for the Life Sciences, Vol. 5) (Weinheim: Wiley-VCH, 2010)
43. Lal S, Link S, Halas N J *Nature Photon.* **1** 641 (2007)
44. Atwater H A, Polman A *Nature Mater.* **9** 205 (2010)
45. Feth N et al. *Opt. Lett.* **33** 1975 (2008)
46. Rockstuhl C et al. *Opt. Express* **16** 2080 (2008)
47. Shahbazyan T V, Stockman M I (Eds) *Plasmonics: Theory and Applications* (Challenges and Advances in Computational Chemistry and Physics, Vol. 15) (Dordrecht: Springer, 2013)
48. Pendry J B et al. *IEEE Trans. Microwave Theory Tech.* **47** 2075 (1999)
49. Linden S et al. *Science* **306** 1351 (2004)
50. Klein M W et al. *Science* **313** 502 (2006)
51. Klein M W et al. *Opt. Express* **15** 5238 (2007)
52. Bethe H A *Phys. Rev.* **66** 163 (1944)
53. Bouwkamp C J *Rep. Prog. Phys.* **17** 35 (1954)
54. García de Abajo F J et al. *Opt. Express* **14** 7 (2006)
55. Roberts A *J. Opt. Soc. Am. A* **4** 1970 (1987)
56. Rindzevicius T et al. *J. Phys. Chem. C* **111** 1207 (2007)
57. Ebbesen T W et al. *Nature* **391** 667 (1998)
58. Garcia-Vidal F J et al. *Rev. Mod. Phys.* **82** 729 (2010)
59. Webb K J, Li J *Phys. Rev. B* **73** 033401 (2006)
60. García-Vidal F J et al. *Phys. Rev. Lett.* **95** 103901 (2005)
61. Lezec H J et al. *Science* **297** 820 (2002)
62. Melentiev P N et al. *Opt. Express* **19** 22743 (2011)
63. Melentiev P N et al. *JETP* **115** 185 (2012); *Zh. Eksp. Teor. Fiz.* **142** 211 (2012)
64. Treshin I V et al. *Phys. Rev. A* **88** 023832 (2013)
65. Yablonovitch E *Phys. Rev. Lett.* **58** 2059 (1987)
66. Notomi M *Rep. Prog. Phys.* **73** 096501 (2010)
67. Carslaw H S, Jaeger J C *Conduction of Heat in Solids* 2nd ed. (Oxford: Clarendon Press, 1959)
68. Schwab K et al. *Nature* **404** 974 (2000)
69. Agraït N, Yeyati A L, van Ruitenbeek J M *Phys. Rep.* **377** 81 (2003)
70. Boyer D et al. *Science* **297** 1160 (2002)
71. Richardson H H et al. *Nano Lett.* **9** 1139 (2009)
72. Baffou G, Girard C, Quidant R *Phys. Rev. Lett.* **104** 136805 (2010)
73. Govorov A O, Richardson H H *Nano Today* **2** (1) 30 (2007)
74. Baffou G, Quidant R, García de Abajo F J *ACS Nano* **4** 709 (2010)
75. Baffou G, Rigneault H *Phys. Rev. B* **84** 035415 (2011)
76. Inouye H et al. *Phys. Rev. B* **57** 11334 (1998)
77. Grua P et al. *Phys. Rev. B* **68** 035424 (2003)
78. Arbouet A et al. *Phys. Rev. Lett.* **90** 177401 (2003)
79. Huang W et al. *J. Phys. Chem. C* **111** 10751 (2007)
80. Hu M, Hartland G V *J. Phys. Chem. B* **106** 7029 (2002)
81. Habenicht A et al. *Science* **309** 2043 (2005)
82. Huang W, Qian W, El-Sayed M A *J. Am. Chem. Soc.* **128** 13330 (2006)
83. Melentiev P N et al. *Laser Phys. Lett.* **10** 075901 (2013)
84. Boyd R W *Nonlinear Optics* 2nd ed. (San Diego, CA: Academic Press, 2003)
85. Fomichev S V et al. *Opt. Express* **11** 2433 (2003)
86. Capretti A et al. *Phys. Rev. B* **89** 125414 (2014)
87. Czaplicki R et al. *Nano Lett.* **15** 530 (2015)
88. Bouhelier A et al. *Phys. Rev. Lett.* **90** 013903 (2003)
89. Kim S et al. *Nature* **453** 757 (2008)
90. Bar-Elli O et al. *ACS Nano* **9** 8064 (2015)
91. Aouani H et al. *Nature Nanotechnol.* **9** 290 (2014)
92. Palomba S, Novotny L *Nano Lett.* **9** 3801 (2009)
93. Danckwerts M, Novotny L *Phys. Rev. Lett.* **98** 026104 (2007)
94. Hajisalem G, Hore D K, Gordon R *Opt. Mater. Express* **5** 2217 (2015)
95. Mooradian A *Phys. Rev. Lett.* **22** 185 (1969)
96. Dulkeith E et al. *Phys. Rev. B* **70** 205424 (2004)
97. Melentiev P N et al. *Opt. Express* **20** 19474 (2012)
98. Ghenuche P et al. *Phys. Rev. Lett.* **101** 116805 (2008)
99. Bouhelier A, Beversluis M R, Novotny L *Appl. Phys. Lett.* **83** 5041 (2003)
100. Schuck P J et al. *Phys. Rev. Lett.* **94** 017402 (2005)
101. Melentiev P N et al. *Opt. Express* **23** 11444 (2015)
102. Melentiev P N et al. *Opt. Express* **21** 13896 (2013)
103. Nezami M S, Gordon R *Opt. Express* **23** 32006 (2015)
104. Guyot-Sionnest P, Chen W, Shen Y R *Phys. Rev. B* **33** 8254 (1986)
105. Butet J et al. *Nano Lett.* **10** 1717 (2010)
106. Metzger B et al. *Nano Lett.* **14** 2867 (2014)
107. Ren M et al. *Nature Commun.* **3** 833 (2012)
108. Genet C, Ebbesen T W *Nature* **445** 39 (2007)
109. Schön P et al. *Opt. Lett.* **35** 4063 (2010)
110. Krause D, Teplin C W, Rogers C T *J. Appl. Phys.* **96** 3626 (2004)
111. Richards B, Wolf E *Proc. R. Soc. Lond. A* **253** 358 (1959)
112. Dadap J I, Shan J, Heinz T F *J. Opt. Soc. Am. B* **21** 1328 (2004)
113. Krasnok A E et al. *Phys. Usp.* **56** 539 (2013); *Usp. Fiz. Nauk* **183** 561 (2013)
114. Kim E M et al. *Phys. Rev. Lett.* **95** 227402 (2005)
115. Konstantinova T Y et al. *Quantum Electron.* **43** 379 (2013); *Kvantovaya Elektron.* **43** 379 (2013)
116. Shalaev V M *Nonlinear Optics of Random Media: Fractal Composites and Metal-Dielectric Films* (Springer Tracts in Modern Physics, Vol. 158) (Berlin: Springer, 2000)
117. Fomichev S V, Zaretsky D F, Becker W *Phys. Rev. B* **79** 085431 (2009)
118. Petrov G I et al. *Appl. Phys. Lett.* **83** 3993 (2003)
119. Wang L et al. *ACS Photon.* **3** 1494 (2016)
120. Hajisalem G, Nezami M S, Gordon R *Nano Lett.* **14** 6651 (2014)
121. Metzger B et al. *ACS Photon.* **1** 471 (2014)
122. Reinhold J et al. *Phys. Rev. B* **86** 115401 (2012)
123. Scalora M et al. *Phys. Rev. A* **82** 043828 (2010)
124. Hanke T et al. *Nano Lett.* **12** 992 (2012)
125. Huang L, Cheng J-X *Annu. Rev. Mater. Res.* **43** 213 (2013)
126. Konstantinova T V et al. *JETP* **117** 21 (2013); *Zh. Eksp. Teor. Fiz.* **144** 27 (2013)
127. Hanke T et al. *Phys. Rev. Lett.* **103** 257404 (2009)
128. Melentiev P N et al. *Opt. Lett.* **38** 2274 (2013)
129. Sasanpour P et al. *Nano* **5** 325 (2010)
130. N'Gom M et al., in *Proc. of the Conf. on Lasers and Electro-Optics/Intern. Quantum Electronics, Baltimore, MD, USA, 2009, OSA Technical Digest* (Washington, DC: Optical Society of America, 2009) paper IMK4
131. Schwartz O, Oron D *Nano Lett.* **9** 4093 (2009)
132. Melentiev P N et al. *Quantum Electron.* **46** 414 (2016); *Kvantovaya Elektron.* **46** 414 (2016)
133. Novotny L, van Hulst N *Nature Photon.* **5** 83 (2011)
134. Castro-Lopez M et al. *Nano Lett.* **11** 4674 (2011)
135. Melentiev P N et al. *Nanotechnology* **20** 235301 (2009)
136. Melentiev P N et al. *Opt. Commun.* **382** 509 (2017)
137. Beversluis M R, Bouhelier A, Novotny L *Phys. Rev. B* **68** 115433 (2003)
138. Boyd G T, Yu Z H, Shen Y R *Phys. Rev. B* **33** 7923 (1986)
139. Durr N J et al. *Nano Lett.* **7** 941 (2007)
140. Dulkeith E et al. *Phys. Rev. B* **70** 205424 (2004)
141. Mohamed M B et al. *Chem. Phys. Lett.* **317** 517 (2000)
142. Shahbazyan T V, Perakis I E, Bigot J-Y *Phys. Rev. Lett.* **81** 3120 (1998)
143. Biagioni P et al. *Nano Lett.* **12** 2941 (2012)
144. Vinogradov A P et al. *Phys. Rev. B* **74** 045128 (2006)
145. Melentiev P, Afanasiev A, Balykin V *Phys. Rev. A* **88** 053841 (2013)
146. Biagioni P, Huang J-S, Hecht B *Rep. Prog. Phys.* **75** 024402 (2012)
147. Novotny L, Hecht B *Principles of Nano-Optics* (Cambridge: Cambridge Univ. Press, 2006)
148. Chon J W M, Iniewski K (Eds) *Nanoplasmonics: Advanced Device Applications* (Boca Raton, FL: CRC Press, 2014)
149. Feise M W, Shadrivov I V, Kivshar Yu S *Phys. Rev. E* **71** 037602 (2005)

150. Tzuang L D et al. *Nature Photon.* **8** 701 (2014)
151. Shaltout A, Kildishev A, Shalaev V *Opt. Mater. Express* **5** 2459 (2015)
152. de Hoop A T *Appl. Sci. Res. B* **8** 135 (1960)
153. Jalas D et al. *Nature Photon.* **7** 579 (2013)
154. Melentiev P N et al. *Eur. Phys. J. D* **71** 152 (2017)
155. Mutlu M et al. *Phys. Rev. Lett.* **108** 213905 (2012)
156. Menzel C et al. *Phys. Rev. Lett.* **104** 253902 (2010)
157. Klimov V V et al. *Phys. Rev. A* **92** 063842 (2015)
158. Kaliteevski M et al. *Phys. Rev. B* **76** 165415 (2007)
159. Vinogradov A P et al. *Phys. Usp.* **53** 243 (2010); *Usp. Fiz. Nauk* **180** 249 (2010)
160. Sarger L, Oberlé J, in *Femtosecond Laser Pulses: Principles and Experiments* (Advanced Texts in Physics, Ed. C Rullière) (Berlin: Springer, 2005) p. 195
161. Mårsell E et al. *Nano Lett.* **15** 6601 (2015)
162. Lange J et al., in *Photonics Europe 2006, Strasbourg, France, 3–7 April 2006* (Bellingham, WA: SPIE Press, 2006) p. 61950Z
163. Auston D H *Appl. Phys. Lett.* **18** 249 (1971)
164. Bowlan P, Gabolde P, Trebino R *Opt. Express* **15** 10219 (2007)
165. Extermann J et al. *Opt. Express* **16** 10405 (2008)
166. Li H et al. *Appl. Phys. Lett.* **96** 021103 (2010)
167. Melentiev P N et al. *Laser Phys. Lett.* **11** 105301 (2014)
168. Gu F X et al. *Nano Today* **2** (3) 14 (2007)
169. Huang X et al. *Lasers Med. Sci.* **23** 217 (2008)
170. Huang X, Neretina S, El-Sayed M A *Adv. Mater.* **21** 4880 (2009)
171. Berns M W et al. *Science* **213** 505 (1981)
172. Yanik M F et al. *Nature* **432** 822 (2004)
173. Timko B T, Dvir T, Kohane D S *Adv. Mater.* **22** 4925 (2010)
174. Selmke M, Braun M, Cichos F *ACS Nano* **6** 2741 (2012)
175. Beard P *Interface Focus* **1** 602 (2011)
176. Robert H M L et al. *ACS Omega* **1** 2 (2016)
177. Deka G et al. *Nanophotonics* **6** (1) 31 (2017)
178. Ashkin A, Dziedzic J M *Science* **235** 1517 (1987)
179. Moffitt J R et al. *Annu. Rev. Biochem.* **77** 205 (2008)
180. Regmi R et al. *Sci. Rep.* **5** 15852 (2015)
181. Novotny L, Bian R X, Xie X S *Phys. Rev. Lett.* **79** 645 (1997)
182. Pang Y, Gordon R *Nano Lett.* **11** 3763 (2011)
183. Chen Y et al. *Opt. Express* **23** 30227 (2015)
184. Gelfand R M, Wheaton S, Gordon R *Opt. Lett.* **39** 6415 (2014)
185. Zehtabi-Oskuie A et al. *Nanotechnology* **25** 495301 (2014)
186. Jones S, Al Balushi A A, Gordon R *J. Opt.* **17** 102001 (2015)
187. Xu H et al. *Nano Lett.* **16** 2639 (2016)
188. Al Balushi A A et al. *Analyst* **140** 4760 (2015)